



7N-02  
198512  
P49

# TECHNICAL NOTE

## D - 247

EXPERIMENTAL INVESTIGATION OF MIXING OF MACH  
NUMBER 3.95 STREAM IN PRESENCE OF WALL

By Marian Visich, Jr., and Paul A. Libby

Polytechnic Institute of Brooklyn

NATIONAL AERONAUTICS AND SPACE ADMINISTRATION  
WASHINGTON

February 1960

(NASA-TN-D-247) EXPERIMENTAL INVESTIGATION  
OF MIXING OF MACH NUMBER 3.95 STREAM IN  
PRESENCE OF WALL (Polytechnic Inst. of  
Brooklyn) 49 p

N89-70892

Unclas  
00/02 0198512

## NATIONAL AERONAUTICS AND SPACE ADMINISTRATION

## TECHNICAL NOTE D-247

## EXPERIMENTAL INVESTIGATION OF MIXING OF MACH

## NUMBER 3.95 STREAM IN PRESENCE OF WALL

By Marian Visich, Jr., and Paul A. Libby

## SUMMARY

W  
1  
3  
2

An experimental investigation of the turbulent mixing of a supersonic stream with a subsonic stream bounded by a wall is described. The Mach number of the mainstream was 3.95 while the mass flow of the secondary stream was varied from zero to a value assuring subsonic flow at the origin of mixing. The difficulties associated with a theoretical treatment of the flow are described first; then the test rig and the testing techniques used to carry out the investigation are discussed. For various mean Mach numbers in the secondary flow, the static pressure distributions along the lower wall and the total head distributions at three downstream stations are presented.

The total-head profiles are interpreted in terms of velocity profiles. These are correlated in terms of an extension to the compressible case of the law of the wall and the law of the wake. The results of such a correlation are discussed.

## INTRODUCTION

In the external flow over high-speed aircraft and missiles and in the internal flow through propulsive devices, there frequently arise fluid-dynamical problems connected with the mixing of streams of different properties, as, for example, different velocities, densities, energies, and composition. Some of these problems, in idealized form, may be considered generalized cases of the classical problem of the mixing at constant pressure of two incompressible homogeneous streams with different velocities. This problem appears to have been treated first by Tollmien in 1926 (ref. 1) and is usually termed "free mixing." There exists extensive literature on this problem and its generalization to compressible, heterogeneous flow (cf., for example, ref. 2).

In other of these current technological problems the idealizations corresponding to free mixing are clearly not applicable. Indeed in many cases the flow field created by the two streams corresponds to the

most general type and involves, for example, equally important pressure and viscous forces, and possibly chemical reactions. Analysis of the flows in these cases is generally not possible. However, there are some flows which are amenable to study and analysis and which are between the highly idealized free-mixing and the complex general case.

It is the purpose of this report to present the results of an experimental investigation of one such flow. The flow is shown in figure 1 schematically and in idealized form. Two streams, denoted by subscripts 1 and 2, are separated by a plate upstream of point O'; the mainstream, corresponding to subscript 1, is of semi-infinite extent while the second stream is bounded by a wall DOE. At point O' the two streams become contiguous and mix. A streamline O'C separates the two streams; the outer edge of the mainstream affected by mixing corresponds to O'A. The edge of the boundary layer corresponding to the secondary flow over the wall DOE is denoted as OB and merges with the lower edge of the mixing zone O'B at B.

Assume now that constant pressure prevails throughout the flow field. It is clear that this flow differs essentially from the usual free-mixing flow. Three regions of interaction between the two streams can be distinguished. In the region closest to the origin of mixing (i.e., point O') there exists an inviscid core of secondary fluid; in this region the interaction of the two viscous regions corresponds to a displacement effect on the mixing region because of the boundary layer on the wall. The second region begins at point B where the inviscid core has been consumed in the two viscous regions. At this point the flow can be considered in terms of a single boundary-layer region with initial profiles of velocity, stagnation enthalpy, and composition. The final region is far downstream from the origin of mixing where the influence of the secondary flow is negligible; in this region the flow corresponds to a boundary layer associated only with the mainstream but with an effective origin upstream of O'.

Flows of the type described here in idealized form arise in a variety of technological problems. For example, consider the problem of isolating a wall or surface (DOE in fig. 1) from a high-energy main flow by means of a low-energy secondary stream. Such schemes have been suggested and studied for combustion chambers and exhaust nozzles in high-performance propulsion devices and for lifting surfaces on aircraft and missiles. The evaluation of such a scheme depends upon the length of adiabatic surface with reduced equilibrium temperature or upon the degree of the heat-transfer reduction realized by a given coolant mass flow. Similar flows also arise in connection with ejectors and engines with a bypass.

In practical problems the idealization inherent in the flow previously described may not be satisfactory. For example, the thickness of

the plate separating the two streams can provide essential pressure disturbances which invalidate the boundary-layer approximation. The effect of the boundary layers on the plate can alter the mixing region significantly. Finally, there may be significant pressure gradients in the mixing and boundary-layer regions; these may be self-induced or associated with outside influences.

The theoretical analysis of the idealized constant-pressure flow appears at the present time to be incomplete. The status of the theoretical analysis of this flow was reviewed in reference 3 and can be summarized as follows: For the incompressible homogeneous case the displacement effect of the boundary layer on the mixing zone in the first region was given for both laminar and turbulent flow in reference 3. The second region can be analyzed from the point of view of the initial profile problem of boundary-layer theory. For the incompressible case this can be stated as follows: At a value of the streamwise coordinate  $x = x_0$  the velocity profile is given as a function of the normal coordinate  $y$ ; the downstream development of this profile must be found. For laminar flow this problem has been the subject of considerable investigation (see ref. 4). It can be stated that only numerical procedures involving stepwise computation for increasing values of  $x$  have been developed to date; adequate approximate but analytic methods of solution are desirable. For the turbulent case no analysis has been carried out; indeed, it is not evident that in general the specification of the velocity profile in terms of mean values is sufficient to permit analysis of downstream behavior. There may be initial profiles which have special characteristics as, for example, those corresponding to the "equilibrium" turbulent layers proposed by Clauser (ref. 5); for these profiles the study of downstream development may be simplified.

For the final region wherein the effect of the secondary flow becomes negligible the usual boundary solutions for both laminar and turbulent flow can be applied. The streamwise coordinate can be adjusted to reflect the approximate effect of the secondary flow.

It is clear from the above discussion that experimental investigation of flows between the highly idealized free-mixing and the complex general case is required. Such a study can simulate more closely the effects of initial boundary layer and thicknesses of the separating plate as well as of compressibility. However, there appear to be several types of data already available which are related to this flow.

For the case of zero secondary flow the problem under consideration is closely related to the flow over a rearward-facing step. The surface downstream of the step is sometimes termed the floor and the effect of various angles between the floor and the surface upstream of the step has been studied. The flow considered herein clearly corresponds to

the case of zero floor angle. The quantities usually measured are the pressure on the step and the pressure distribution on the floor. The parameters, other than floor angle, are the Mach number at the step, the character and thickness of the boundary layer at the edge of the step, and the height of the step. Such data at various Mach numbers have been provided by Eggink (ref. 6), Goin (ref. 7), and Chapman, Kuehn, and Larson (ref. 8). Many of these data have been reviewed and compared with a theoretical analysis by Korst in reference 9. In research as yet unpublished Bogdonoff has carried out tests at free-stream Mach numbers upstream of the step of 2.31 and 2.87<sup>1</sup>.

With secondary flow the flow field is related to that involved in the use of base bleed to reduce base pressure. Wimbrow (ref. 10) has provided data for this case. The measured quantities are the base pressures as functions of secondary mass flow, while the parameters are the geometry of the base region, the Mach number of the mainstream, and the boundary-layer characteristics at the edge of the base. It is clear that exact correspondence is not achieved in these tests since the influence of the shear stresses and of the constraint of the floor or wall is not present.

The experimental research reported herein involved an investigation of the two-dimensional mixing of a main stream at a Mach number of 3.95 and of a subsonic secondary stream. The two streams were of essentially the same energy. The boundary layer at the origin of mixing was turbulent with a ratio of initial boundary-layer thickness to step height of approximately 1/3. The pressure distributions along the floor and the total head profiles at several downstream stations with and without a secondary stream mass flow were measured.

This work, carried out at the Polytechnic Institute of Brooklyn Aeronautical Laboratories, was sponsored by and conducted with the financial assistance of the National Advisory Committee for Aeronautics. The authors are pleased to acknowledge the invaluable contributions to the research of Professor Antonio Ferri, who suggested the investigation and provided valuable advice. Mr. George Gaitatzes, Research Assistant, helped carry out the test program.

#### SYMBOLS

A,B	empirical constants of logarithmic velocity profile; A = 2.5; B = 5.1.
h	sum of splitter-plate thickness and height of secondary stream, 0.36 in.

---

<sup>1</sup>The authors gratefully acknowledge receipt from Professor S. M. Bogdonoff of the results of this research prior to publication.

M	Mach number
$\bar{M}_2$	mean Mach number of secondary flow at origin of mixing
$P_b$	base pressure coefficient, $(P_b - P_1)/q_1$
p	static pressure
$p_b$	base pressure
$p_t$	stagnation pressure
q	dynamic pressure
u	velocity component parallel to wall in x-direction
$v^*$	shearing velocity, $\sqrt{\tau_w/\rho_w}$
W	wake function, $W(\eta)$
x,y,z	Cartesian coordinates with origin on lower wall (fig. 1)
X	transformed x-coordinate, $\int_0^x \sqrt{\rho_e/\rho_w} (\mu_e/\mu_w) dx$
$\delta$	boundary-layer thickness
$\eta = y/\delta$	
$\bar{\eta} = \int_0^y (\rho/\rho_w) dy / \int_0^\delta (\rho/\rho_w) dy$	
$\mu$	coefficient of viscosity
$\nu$	coefficient of kinematic viscosity
$\rho$	mass density
$\xi = v^* \int_0^y (\rho/\rho_w) dy / \nu_w$	
$\Pi$	function of streamwise coordinate x, in general unknown
$\tau_w$	wall shear stress

## Subscripts:

- 1 flow conditions of mainstream at origin of mixing
- 2 flow conditions of secondary stream at origin of mixing
- e conditions at outer edge of boundary layer,  $y = \delta$
- w conditions at wall,  $y = 0$

## TEST APPARATUS AND TESTING TECHNIQUES

To investigate experimentally the flow previously described the special test rig shown in figure 2 was designed, constructed, and utilized in conjunction with a blowdown wind tunnel. The air supply and related equipment involved are described in reference 11. Photographs of the rig in place are given in figure 3.

## Test Rig and Test Conditions

A half nozzle with a nominal exit Mach number of 4.2 and a nominal test section 2 inches high and 8 inches in width was used to establish the mainstream. The large ratio of width to height was dictated by the necessity of establishing two-dimensional flow along the centerline. The flow in the nozzle was supplied from a settling chamber 3 feet in diameter and capable of operating at pressures up to 600 psia. A rectangular channel was attached downstream of the nozzle. The secondary flow was introduced parallel to the lower wall of this channel and was separated from the mainstream by a splitter plate. Air for the secondary flow was obtained from the same air supply as the main stream but was controlled independently. The mass flow of the secondary stream was metered by means of a sonic orifice before it was introduced into its settling chamber.

The parameters which could be varied in this test setup are stagnation pressure of the two streams, thickness of the splitter plate, and height of the secondary stream at the origin of mixing. With little modification the secondary stream could be supplied with a gas different from air so that flows with diffusion could be investigated. For the tests reported herein fixed values of mainstream stagnation pressure, splitter-plate thickness, and height of the secondary stream were chosen; thus the only parameter varied was the stagnation pressure of the secondary stream.

The thickness of the splitter plate and the height of the secondary stream at the origin of mixing were 0.11 and 0.25 inch, respectively. The total cross-sectional area of the channel at the origin of mixing was  $2.85 \times 8$  inches. The upper wall of the channel was diverged approximately  $2^\circ$  from the lower wall.

The tests were carried out at a mainstream stagnation pressure of 320 psia. At the corresponding Reynolds number the actual mainstream Mach number, as determined from the static pressure and Mach waves in the mainstream, was found to be 3.95. The secondary mass flow was varied from zero to a value assuring subsonic flow in the secondary flow at the origin of mixing. If higher secondary mass flows had been used the secondary stream would have become sonic or supersonic at the origin of mixing and a complex wave pattern throughout the downstream viscous region would have developed. In order to keep the experimental conditions close to those of the idealized flow shown in figure 1, these higher rates of secondary mass flow were not investigated.

The mass flow in the two streams was relatively small compared with that available from the air supply, and the stagnation temperatures of the two streams were essentially the same, were close to ambient, and were only slowly varying during the test runs. This behavior was established from stagnation-temperature probes in the two settling chambers and from thermocouples in the lower wall of the channel. During several preliminary tests continuous temperature recordings were made and were found to differ by only  $20^\circ$  to  $30^\circ$  F. For data reduction it was therefore assumed that the test conditions corresponded to zero heat transfer and to isoenergetic flows with stagnation temperatures of  $500^\circ$  R.

The Reynolds number in the main stream was clearly high enough to induce fully developed turbulent flow at the origin of mixing. Although no survey of the boundary layer at this station was made, the thickness of the boundary layer was estimated to have been 0.12 inch.

Because of the high pressure of the main stream and the sensitivity of the test results to leakage between streams and between the exterior and the passage, considerable attention was devoted to sealing the many contact surfaces in the rig.

#### Measurements Performed

Measurements were made of the static-pressure distribution along the lower wall of the passage and of the total-head profile at three stations downstream of the origin of mixing. Because of the high stagnation pressure of the mainstream and the necessity of minimizing the flow disturbance due to the total-head survey rake, designing the rake presented some difficulties. After several trials the design shown in

figure 4 was chosen. The rake was supported primarily from the upper wall of the channel with light, sweptback struts at its downstream lower edge. The tubes nearest the lower wall were extended down and forward from the main body of the rake.

Total-head surveys were carried out at three downstream stations located by the ratio  $x/h$ , where  $x$  is the distance parallel to the lower wall measured from the origin of mixing and  $h$  is the sum of the splitter plate thickness and the height of the secondary stream and equal to 0.36 inch. (For the case of zero secondary flow,  $h$  corresponds to the step height.) The three stations are at  $x/h = 12.8$ , 18.4, and 29.4. The rake was set in several different vertical positions; the position closest to the lower wall was the position which showed no interference between the rake and the flow. This was determined by comparing the total-head data given by the position of the rake under consideration with that given by the adjacent upward position of the rake. For the most part surveys were performed on the centerline of the channel; however, one survey was carried out at the most downstream station and offset from the centerline 1 inch in order to establish the two-dimensionality of the flow.

The stations for the total-head surveys were selected to correspond to regions within which the boundary-layer approximation was closely satisfied and the flow was two dimensional. The most upstream position was therefore dictated by the position of the oblique shock and the associated compression zone which turns the flow parallel to the lower wall. The most downstream position for a total-head survey was suggested by the position of the Mach waves from the intersections of the splitter plate and the side walls of the channel.

The static pressure on the lower surface of the channel was measured along the centerline of the channel and along lines normal to the centerline at  $x/h = 5.6$  and 22.2. Again the lateral distributions were used to establish the two dimensionality of the flow.

Pressures in the range of 30 psia or higher were measured on Heise gages and recorded photographically. Lower pressures were measured on a multiple-tube mercury manometer and also recorded photographically. In a typical test the stagnation pressure of the main stream was established first at 322 psia; then the desired secondary mass flow as indicated by the stagnation pressure ahead of the flowmeter was established. After steady conditions for these two pressures had been obtained, a series of photographs of the pressure instrumentation were taken. The steadiness of the indication was established by viewing successive pictures. Schlieren photographs with knife edge parallel to the flow were also taken during most tests.

### Estimated Measurement Accuracy

The overall accuracy of the pressure measurements can be summarized as follows:

Instrument	Pressure range	Accuracy
Heise gage	0 to 600 psig	$\pm 1$ psi
Heise gage	0 to 250 psig	$\pm 1$ psi
Heise gage	0 to 200 psig	$\pm .5$ psi
Heise gage	0 to 100 psig	$\pm .25$ psi
Mercury manometer	0 to 60 in. Hg gage	$\pm .1$ in. Hg

It was possible to set the stagnation pressure of the mainstream within  $\pm 2$  psi of the mean stagnation pressure of 322 psia. The stagnation pressure ahead of the flowmeter, which measured the mass flow passing through the secondary stream, reached a maximum value of 70 psia for  $\bar{M}_2 = 0.44$ . It was possible to set the stagnation pressure ahead of the flowmeter within  $\pm 0.25$  psi of the desired value.

### PRESENTATION AND DISCUSSION OF DATA

The value of the secondary mass flow has been specified in terms of a mean Mach number  $\bar{M}_2$  at the origin of mixing. This was obtained from the measured mass flow and the static pressure in the secondary stream near the origin of mixing. The maximum value of  $\bar{M}_2$  is 0.44.

For the presentation of data it is convenient to locate a Cartesian coordinate system at the intersection of the centerline of symmetry of the channel, the lower wall, and the end of the splitter plate. The x-coordinate is measured in the streamwise direction, the y-coordinate normal to the lower wall, and the z-coordinate orthogonal to the other two, parallel to the edge of the splitter plate. All dimensions have been nondimensionalized with respect to  $h$ , which is equivalent to the step height for zero secondary flow.

### Two Dimensionality of Flow

The static pressure distributions with  $z/h$  in terms of the pressure ratio  $p/p_{t1}$  are shown in figure 5 for various values of  $\bar{M}_2$  and  $x/h$ . In figure 6 are shown the stagnation pressure profiles for the two values of  $z/h$  and for  $x/h = 29.42$ , the most downstream position at

which velocity profiles were measured. From figure 6 it is concluded that within measuring accuracy the flow is two dimensional along the centerline of symmetry.

### Pressure Distribution on Lower Wall

In figure 7 the effect of secondary mass flow on the pressure distributions along the lower wall of the channel is shown. Also shown are the theoretical asymptotic values of the static pressure computed on the basis of an isentropic expansion and compression of the main stream; these theoretical values correspond to  $p_1/p_{t1} = 0.00704$ . There do not appear to be any directly comparable data in the literature. However, for the special case of  $\bar{M}_2 = 0$ , the distributions of reference 8 at a free-stream Mach number  $M_1 = 2.0$  and the unpublished data of Bogdonoff at  $M_1 = 2.31$  and  $2.91$  are shown in figure 8. As might be expected, the effect of increasing  $M_1$  is to increase the distance from the origin at which the pressure reaches a constant value.

The static pressure  $p_1$  for zero secondary mass flow can also be compared with the available two-dimensional base-pressure data. For this purpose the compilation of reference 7 along with the present datum point and the estimated variation of reference 12 are shown in figure 9. It will be noted that the measured value appears to be somewhat lower than the estimated value of reference 12. This might be accounted for by any one or a combination of the following three deviations from the conditions usually extant for base-pressure measurements: (1) The relatively thick boundary layer at the edge of the step, (2) the absence of geometric restraint on the step, or (3) the presence of the floor. Also shown in figure 9 are the data available from reference 10 and from Bogdonoff (unpublished data); the former are obtained without the floor and the latter, with a ratio of boundary-layer thickness to step height close to that prevailing in the tests here. Also shown are the data of references 8 and 13. From the Reynolds number and schlieren pictures given in reference 8 it appears that the ratio of boundary-layer thickness to step height is much smaller than that which prevailed in these tests. From a comparison of these results it appears that the opening at the step results in the reduced base pressure; another manifestation of this opening is discussed below.

The effect of secondary mass flow on the pressure  $p_2$  can be shown in terms of a representation close to that given in reference 10. This is given in figure 10 where the pressure ratio  $p_2/p_1$  is shown as a function of  $p_{t2}/p_1$ . The line  $p_2 = p_{t2}$  corresponds to the case of

zero flow; it will be noted, however, that the pressure  $p_2$  is actually greater than  $p_{t2}$  for this case. Careful checking of all pressure seals and of all measurements established that the pressure  $p_2$  was indeed greater than  $p_{t2}$ . This result can be accounted for by a vortex near the exit of the secondary flow and within the settling chamber; this vortex results in the low base pressure discussed above.

With a small secondary mass flow the pressure  $p_2$  increases greatly; this corresponds to the observed sensitivity of base pressure to small base bleed as shown in reference 10. Also similar to the results shown in reference 10 is the insensitivity of the pressure  $p_2$  to increases in secondary weight flow beyond a relatively small value ( $\bar{M}_2 \approx 0.20$ ).

#### Total-Head Profiles

The total-head profiles at various secondary mass flows and various downstream stations are shown in figure 11. The data of figure 6 should also be considered to complete the presentation of data related to total-head profiles.

#### Schlieren Photographs

In figure 12 the schlieren pictures corresponding to various values of  $\bar{M}_2$  and to the rake in its most downstream position are shown. These pictures are composites of three separate schlieren photographs taken during three separate tests at the same value of  $\bar{M}_2$ .

Several comments can be made concerning these photographs. The general features of the flow are the same for all values of  $\bar{M}_2$ ; the mainstream flow expands at the origin of mixing and then recompresses through a compression zone in the neighborhood of  $x/h \approx 6$  to 8. The height of the mixing zone between the two streams increases and the amount of expansion of the mainstream at the origin of mixing decreases as  $\bar{M}_2$  increases. The presence of a second family wave from the upper wall of the channel will be noticed. This wave originated at the junction of the nozzle and the channel. The ratio of  $\Delta p/q_1$  for this wave was estimated from pressure measurements on the upper wall to be less than 1 percent. It is, however, possible that this wave leads to some distortion of the outer portion of the boundary-layer profiles at  $x/h = 29.4$  despite the fact that it did not affect the static pressure as measured on the lower wall. (Although the presence of this wave was

known early in the investigation, its weakness lead to the possibly faulty assumption that it would not significantly affect the boundary layer on the lower wall.)

Figure 13 is a photograph of the flow field near the origin of mixing for  $\bar{M}_2 \approx 0.50$ . This is presented to indicate the more complex flow pattern resulting for the larger values of  $\bar{M}_2$ . Similar results are shown in reference 10.

## INTERPRETATION OF TOTAL-HEAD PROFILES

### IN TERMS OF VELOCITY PROFILES

In this section the total-head profiles presented previously are reduced to velocity profiles which are then interpreted in terms of the concept of the law of the wall and the law of the wake generalized to compressible flow. Such an interpretation may be of value in connection with a theoretical analysis of the boundary-layer development downstream of the recompression zone.

The total-head profiles can be interpreted in terms of velocity profiles within a boundary layer provided the flow is assumed to be adiabatic and the static pressure normal to the wall, to be constant. The adiabatic assumption has been discussed above and the static-pressure assumption is believed reasonable because of the relatively small thickness of the layer.

The theoretical basis for an analysis of these profiles is provided by Mager (ref. 14). By applying the transformations well known to laminar compressible boundary-layer theory, Mager reduced the partial differential equations for the compressible turbulent boundary layer to an incompressible form provided the turbulent Prandtl number is unity, the flow is adiabatic, and the turbulent shear stresses per unit mass are invariant under the transformations. This reduction has been recently generalized by Vaglio-Laurin to the case of heat transfer (ref. 15).

The direct reduction of the turbulent compressible equations to incompressible form suggests a correlation of the velocity profiles of this report in terms of the variables used by Coles (refs. 16 and 17) for incompressible turbulent flows. By carefully considering a large number of turbulent velocity profiles measured by many investigators under conditions of constant pressure as well as of favorable and adverse pressure gradients, Coles established the following useful correlation:

$$\frac{u}{v^*} = A \log_e \frac{yv^*}{v} + B + A\Pi(x)W(\eta) \quad (1)$$

Equation (1) is a generalization of two of the well-known laws used in turbulent analyses: the logarithmic velocity profile, known to be applicable in the portion of the boundary layer adjacent to the wall, and the velocity-defect law, known to be applicable away from the wall. In the equilibrium turbulent boundary layers of Clauser (refs. 5 and 18) the function  $\Pi$  is constant. Thus for constant-pressure boundary layers  $\Pi = 0.55$ ; for favorable pressure gradients  $0 < \Pi < 0.55$ ; and for the adverse case  $\Pi > 0.55$ . In the boundary layer with a general pressure distribution there appears at the present to be no analysis permitting the determination of  $\Pi(x)$ . It will be noted that the profiles represented by equation (1) are a two-parameter family corresponding to  $v^*(x)$  and  $\Pi(x)$ . Theoretical analyses of the turbulent boundary layer have been devoted almost exclusively to one-parameter representations of the velocity profile and are not applicable to the more general profiles discussed here.

In connection with the problem of the mixing of two streams in the presence of a wall, it is of interest to consider the correlation of the velocity profiles in terms of equation (1) which has been generalized to compressible flow by application of the aforementioned transformations. In making this correlation no consideration is given to the question of the theoretical determination of  $\Pi(x)$  or of the uniqueness of the turbulent boundary layer specified in terms of mean values. Thus in this respect a pragmatic point of view is adopted.

The generalization of equation (1) to the compressible adiabatic case on application of the transformations in reference 14 results in the equation:

$$\frac{u}{v^*} = A \log_e \frac{v^* \int_0^y (\rho/\rho_w) dy}{v_w} + B + A\Pi(X)W(\bar{\eta}) \quad (2)$$

where  $v_w \equiv \mu_w/\rho_w$  is the kinematic viscosity at wall conditions,  $W(\bar{\eta})$  is the wake function tabulated in reference 16, and the other symbols are defined in the symbol list. In correlating the velocity profiles given as  $u = u(y)$  in terms of equation (2), it is necessary to find the values of  $v^*$ ,  $\Pi$ , and  $\delta$  providing agreement therewith.

A comment concerning the density at the wall  $\rho_w$  is of interest. In the correlation presented here the value of  $\rho_w$  was taken to be that

corresponding to a wall temperature of 500° R rather than to an adiabatic wall temperature. This is justified on the grounds of: (1) Consistency with the unity turbulent Prandtl number required by the transformations applied by Mager; (2) closeness of the actual wall temperature to this value, and (3) ignorance of the turbulent recovery factor for turbulent boundary layers of the type existing on the wall under consideration. It is possible that heat-transfer investigations under similar conditions could provide values of  $\rho_w$  which would modify somewhat the correlation presented here.

For a given profile a guided trial-and-error procedure was followed in the determination of  $v^*$ ,  $\Pi$ , and  $\delta$ . First, it was necessary to obtain a reasonable estimate for the integral  $\int_0^y (\rho/\rho_w) dy$  for values of  $y < y_0$  where  $y_0$  is the smallest value of  $y$  for which the velocity is determined from experimental data. For this purpose the  $\Pi(x)$  term in equation (2) is neglected for  $\bar{\eta} \ll 1$  and an iteration procedure is applied; an assumption of  $\rho/\rho_w$  as a function of  $y$  for  $y < y_0$  permitted an estimate to be made of  $v^*$  from equation (2) with  $\Pi = 0$  from the measured velocities in the neighborhood of  $y \geq y_0$ . Thus a new  $\rho/\rho_w$  distribution could be determined and the process repeated until  $v^*$  was essentially unchanged. In this manner the experimental data could be represented as  $u = u(\xi)$  where  $\xi \equiv v^* \int_0^y (\rho/\rho_w) dy / v_w$ .

The next step was to estimate  $\delta$  from the profile data. For this it was necessary to consider the profiles of the total pressure ahead of the total-head tubes;  $\delta$  was determined from the measured total-head pressures and the static pressure on the wall. From this total head a more reasonable estimate for  $\delta$  could be made than from the velocity profiles. Then a least-square procedure was applied to equation (2) to determine  $v^*$  and  $\Pi$ . The points near the outer edge of the boundary layer were in some cases weighted to reflect the number of free-stream points measured. When values of  $v^*$  and  $\Pi$  had been computed the estimates of  $v^*$  and  $\delta$  previously made were reviewed and adjusted as required.

The results of this procedure are shown in figure 14 where the profiles  $u/v^*$  versus  $\xi$  for nominal constant values of  $M_2$  are presented. Associated with each profile are the indicated values of  $v^*$ ,  $\Pi$ , and

$\xi_e \equiv v^* \int_0^\delta (\rho/\rho_w) dy / v_w$ . Shown in figures 15 and 16 are the distributions

of  $\Pi$  and  $v^*$  as functions of  $(X - X_0)/h$  where  $X_0$  denotes the unknown value of  $X$  corresponding to the first measuring station ( $x/h = 12.8$ ).

Consider the resulting correlations. It is of interest to note that the experimental profiles can be reasonably correlated by equation (2). Moreover, as might be anticipated on physical grounds, the wake contribution measured by  $\Pi$  decreases in the downstream direction while the local shearing stress at the wall as indicated by  $v^*$  increases. Several comments concerning this correlation are in order. The values of  $v^*$  obtained from the correlation can be used in the two-dimensional boundary-layer equation in integral form to determine if consistent values of momentum thickness are obtained. In carrying out this check for a given value of  $\bar{M}_2$ , the experimental value of the momentum thickness at the most upstream position ( $x/h = 12.8$ ) can be used as an initial value and the experimental values of the form factor can be used to complete the specification of the problem. The results of this check indicate that the experimental values of  $v^*$  are consistent within the experimental accuracy with the equation of motion and with the measured values of momentum thickness.

For the zero secondary flow and the most downstream measuring station, a negative value of  $\Pi$  is obtained, and for the smaller secondary flows values of  $\Pi$  less than 0.55 are obtained. On the basis of the analyses of incompressible flows by Coles and the transformations applied by Mager such values may not appear reasonable. There appear to be two possible explanations for these low values of  $\Pi$ . One explanation is that these results may indicate an influence of the weak compression wave from the upper wall of the channel on the outer portion of the boundary layer. Because of its contribution of a velocity component normal to the wall, such a wave would have the effect of reducing the wake contribution to the velocity profile and therefore reducing the value of  $\Pi$ . To clarify this possibility or to determine if indeed the values of  $\Pi$  are correct, additional tests with this wave eliminated would have to be performed.

Another explanation for the low values could be the effect of the upstream history of the wake portion of the boundary. It will be realized that the outer portion of the turbulent boundary, which has a longer response time (cf. ref. 5), could be significantly altered by the expansion and recompression encountered downstream of the splitter plate. As a result the value of  $\Pi$  in a local region of almost constant pressure may be different from that which would prevail in an extensive region of almost constant pressure.

The correlation of the velocity profiles in terms of equation (2) is not directly applicable to the theoretical estimation of the

downstream development of a boundary layer with a specified initial value of  $\Pi$ . For this estimation an additional relation beyond the usual boundary-layer equations must be available to complete the system of equations and unknowns. Thus the status of the theoretical analysis of the boundary layers considered here is essentially the same as that for the incompressible case; as mentioned previously there is no method for predicting  $\Pi(x)$  for a general pressure distribution. In some examples the two-layer model of the turbulent boundary layer suggested by Clauser (ref. 5) and others may be applicable; additional experimental and theoretical research on turbulent boundary layers involving more than one parameter is required.

#### CONCLUDING REMARKS

An experimental investigation of the mixing of a supersonic mainstream and a subsonic secondary stream in the presence of a wall has been carried out. The secondary flow was between the main flow and the wall. The Mach number of mainstream ahead of the origin of mixing was 3.95. The pressure distributions along the wall were measured for various rates of secondary mass flow and were compared with existing data. Total-head profiles at three downstream stations were also measured.

The total-head profiles were used in connection with the static pressure measured along the lower wall to obtain velocity profiles. These were correlated in terms of an extension of the law of the wall and the law of the wake to compressible flow. Satisfactory correlation was obtained although the values of the function measuring the wake contribution at the most downstream station may have been affected somewhat by a spurious weak compression wave from the opposite wall. Additional theoretical and experimental work would be required in order to establish a convincing theoretical treatment of the flow which was studied experimentally in the research reported here.

Polytechnic Institute of Brooklyn,  
Brooklyn, N.Y., January 5, 1959.

## REFERENCES

1. Tollmien, W.: Berechnung der Turbulenten Ausbreitungsvorgänge. Zamm, Bd. 6, Heft 6, Dec. 1926, p. 468-478. (Also available as NACA TM 1085.)
2. Pai, S.: Fluid Dynamics of Jets. D. Van Nostrand Co., Inc. (New York), 1954.
3. Napolitano, L. G., Libby, P. A., and Ferri, A.: Recent Work on Mixing at the Polytechnic Institute of Brooklyn. Third AGARD Colloquium on Combustion and Propulsion (Mar. 17-21, 1958, Palermo, Sicily), Pergamon Press, 1958, pp. 118-152.
4. Schlichting, H.: Boundary Layer Theory. McGraw-Hill Book Co., Inc., 1955, pp. 150-153.
5. Clauser, F.: The Turbulent Boundary Layer. Vol. IV of Advances in Applied Mechanics, Academic Press, Inc. (New York). Richard von Mises and Theodore von Kármán, eds., 1956, pp. 2-52.
6. Eggink, H.: The Improvement in Pressure Recovery in Supersonic Wind Tunnels. R&M No. 2703, British A.R.C., 1953.
7. Goin, K. L.: Effect of Plan Form, Airfoil Section, and Angle of Attack on the Pressures Along the Base of Blunt-Trailing-Edge Wings at Mach Numbers of 1.41, 1.62, and 1.96. NACA RM L52D21, 1952.
8. Chapman, D. R., Kuehn, D. M., and Larson, H. K.: Investigation of Separated Flows in Supersonic and Subsonic Streams with Emphasis on the Effect of Transition. NACA Rep. 1356, 1958. (Supersedes NACA TN 3869.)
9. Korst, H. H.: A Theory for Base Pressures in Transonic and Supersonic Flow. Jour. Appl. Mech., vol 23, no. 4, Dec. 1956, pp. 593-600.
10. Wimbrow, W. R.: Effects of Base Bleed on the Base Pressure of Blunt-Trailing-Edge Airfoils at Supersonic Speeds. NACA RM A54A07, 1954.
11. Libby, P. A., and Bloom, M. H.: Facilities for Experimental High Speed Aerodynamic Research at the Polytechnic Institute of Brooklyn. Proc. Conf. High Speed Aeronautics, Polytechnic Inst. of Brooklyn, 1955, pp. 363-375.

12. Love, E. S.: Base Pressure at Supersonic Speeds on Two-Dimensional Airfoils and on Bodies of Revolution With and Without Fins Having Turbulent Boundary Layers. NACA TN 3819, 1957. (Supersedes NACA RM L53C02.)
13. Chapman, Dean R.: An Analysis of Base Pressure at Supersonic Velocities and Comparison with Experiment. NACA Rep. 1051, 1951.
14. Mager, A.: Transformation of the Compressible Turbulent Boundary Layer. Jour. Aero. Sci., vol. 25, no. 5, May 1958, pp. 305-311.
15. Vaglio-Laurin, R.: Turbulent Heat Transfer on Blunt-Nosed Bodies in Two-Dimensional and General Three-Dimensional Hypersonic Flow. WADC TN 58-301, AD 206 050, Sept. 1958.
16. Coles, D.: The Law of the Wake in the Turbulent Boundary Layer. Jour. Fluid Mech., vol. 1, pt 2, July 1956, pp. 191-226.
17. Coles, D.: Remarks on the Equilibrium Turbulent Boundary Layer. Jour. Aero. Sci., vol 24, no. 7, July 1957, pp. 495-506.
18. Clauser, F.: Turbulent Boundary Layers in Adverse Pressure Gradients. Jour. Aero. Sci., vol. 21, no. 2, Feb 1954, pp. 91-108.

W  
1  
3  
2

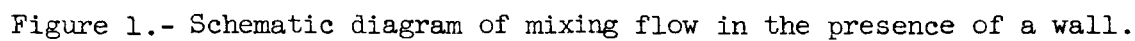


Figure 1.- Schematic diagram of mixing flow in the presence of a wall.

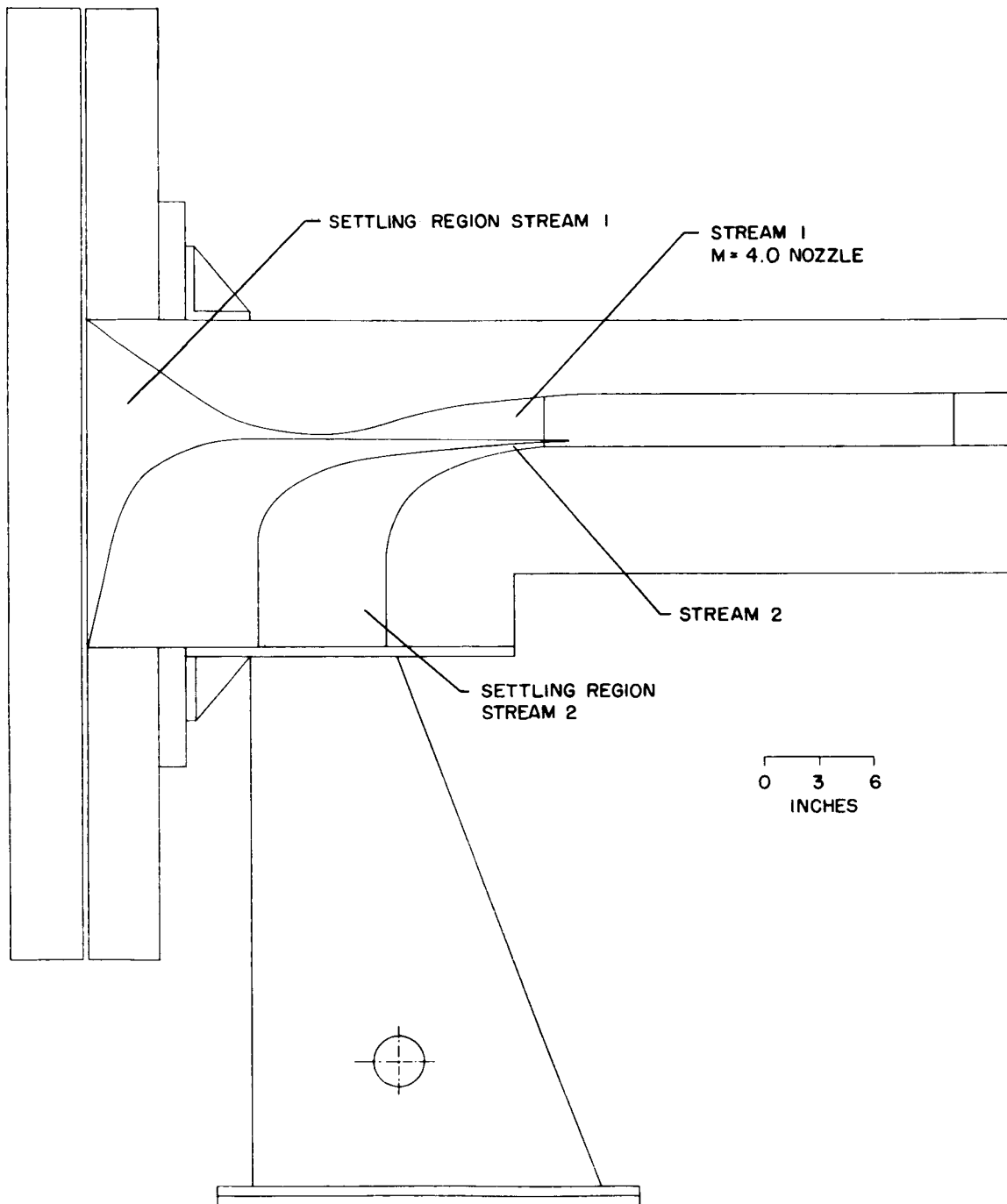
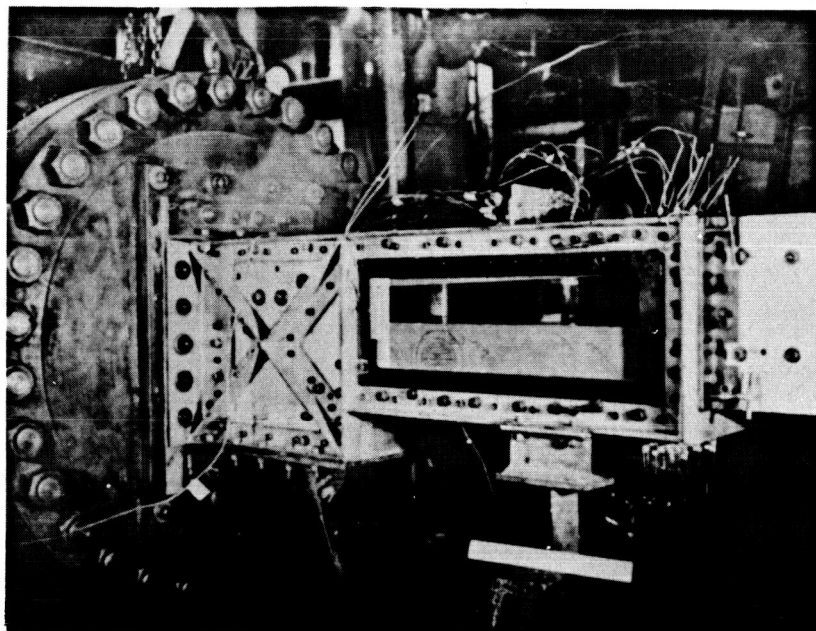
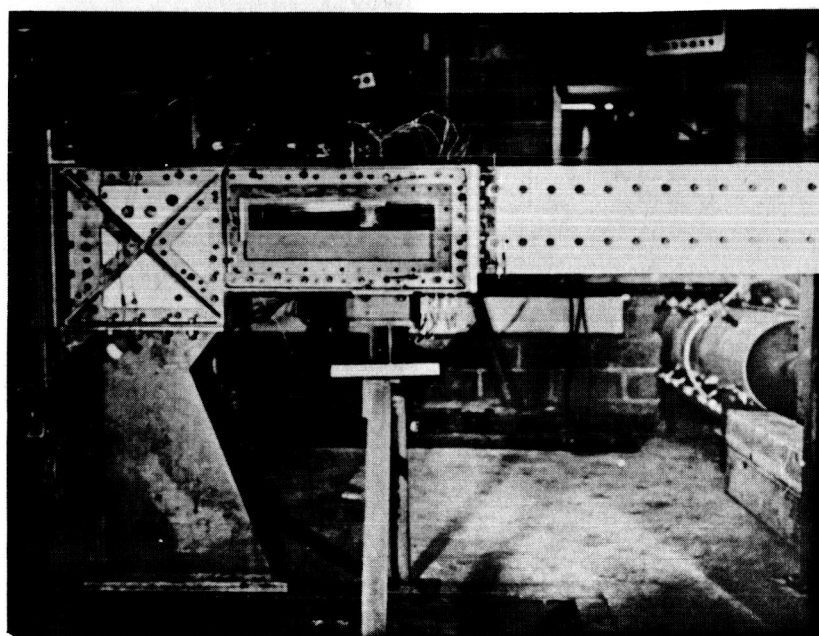


Figure 2.- Schematic diagram of test rig.



(a) Quarter view looking upstream.



(b) Side view.

L-59-6465

Figure 3.- Photographs of test rig.

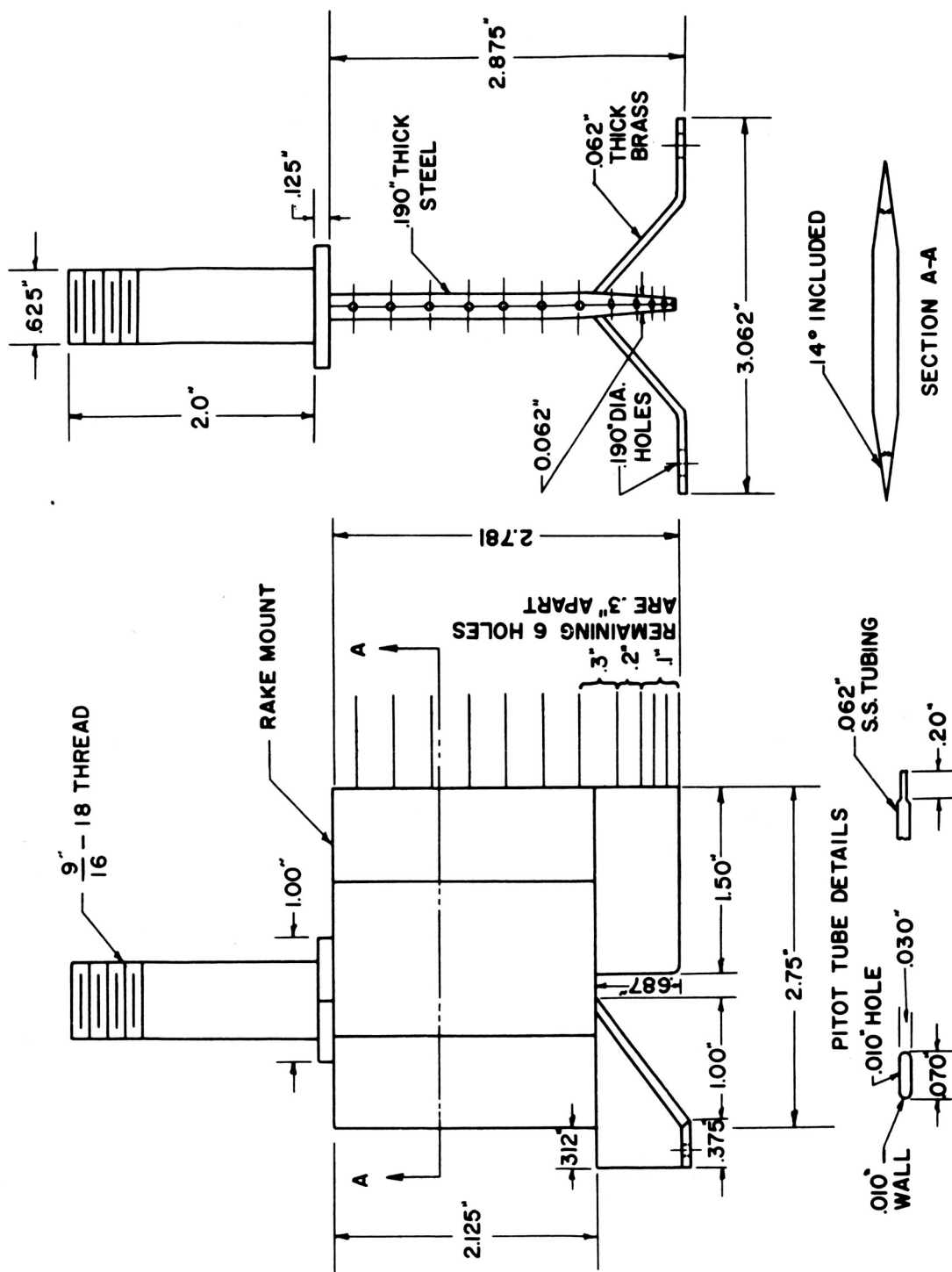
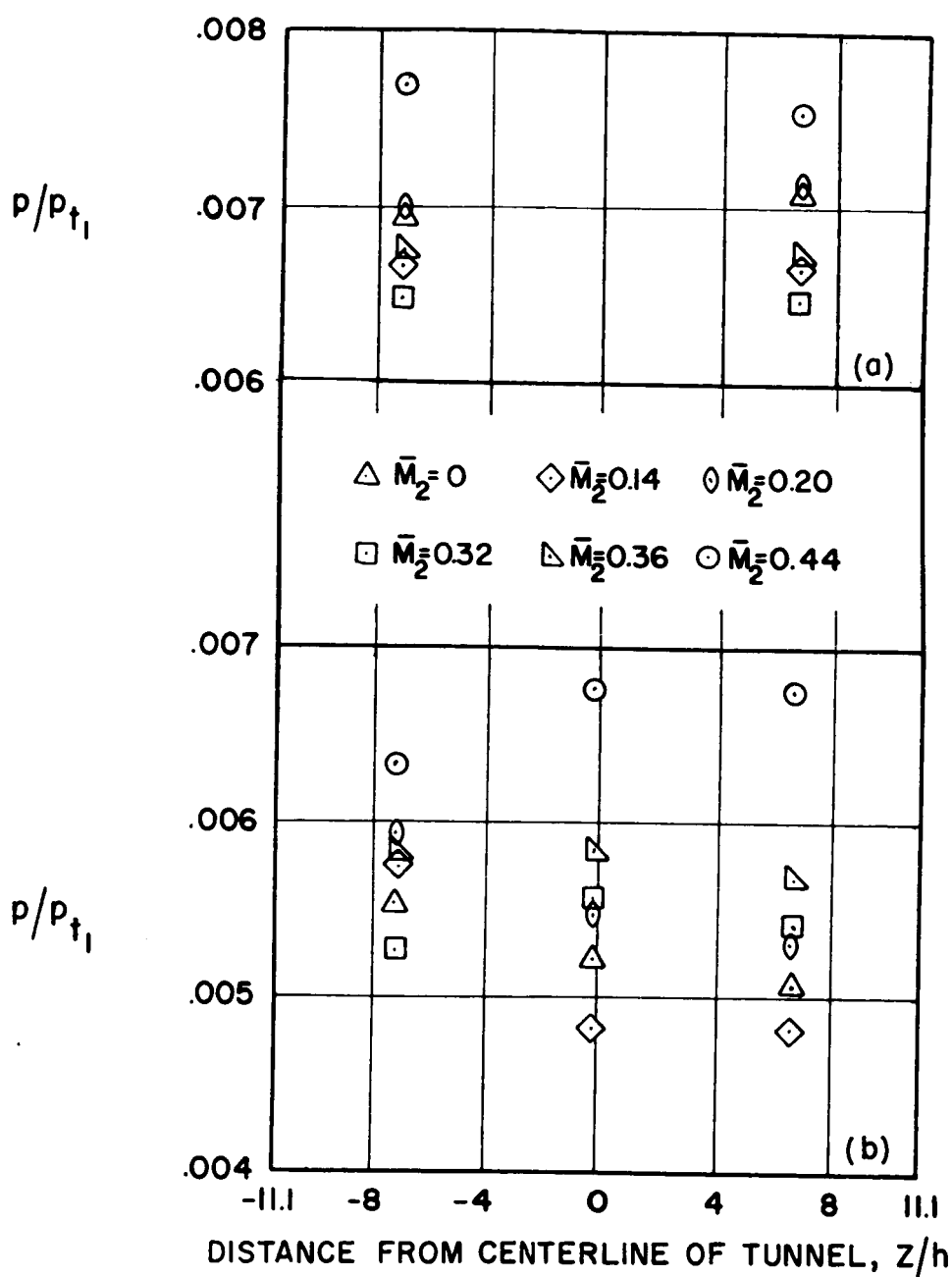


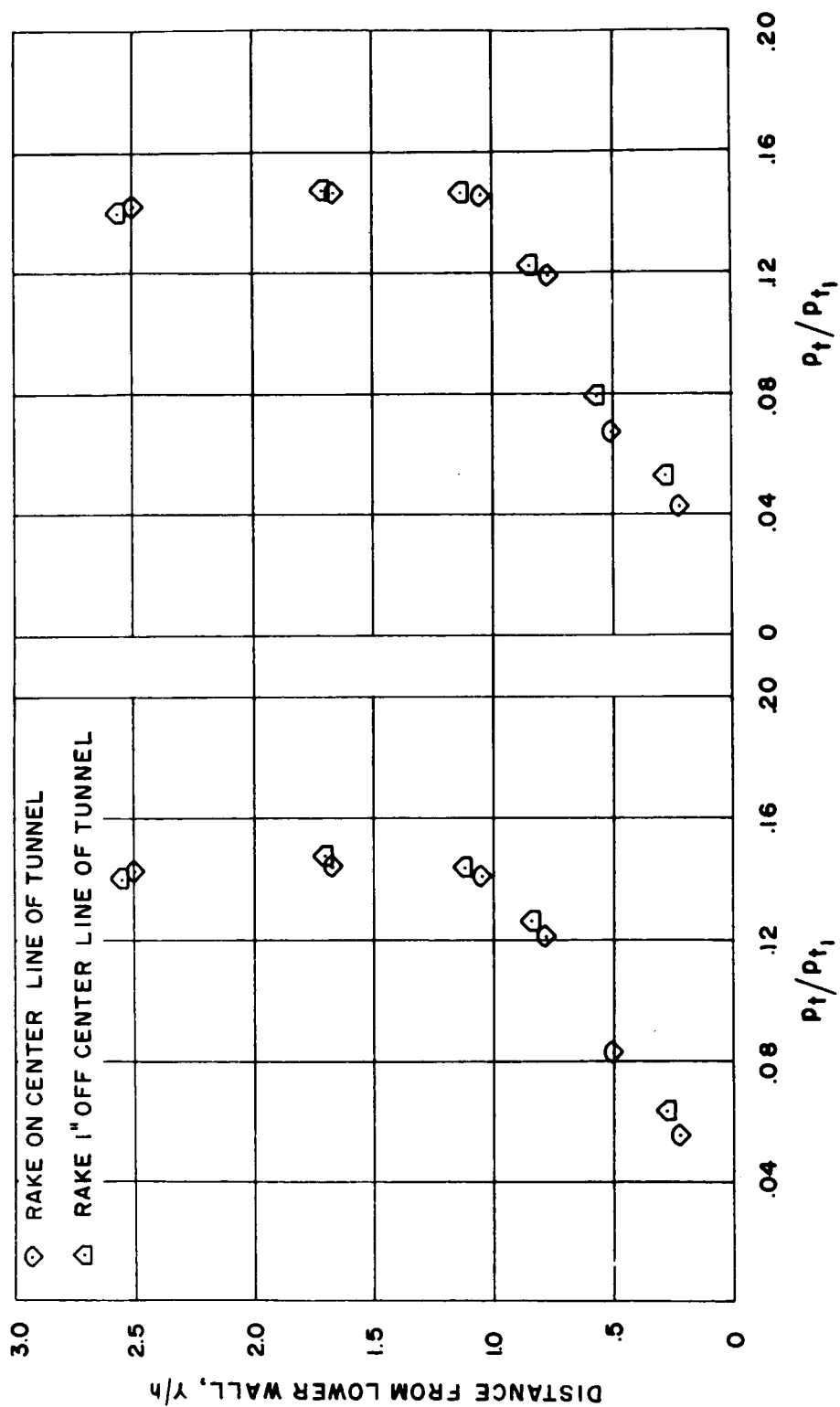
Figure 4.- Total-head survey rake.



(a)  $x/h = 22.22$ .

(b)  $x/h = 5.55$ .

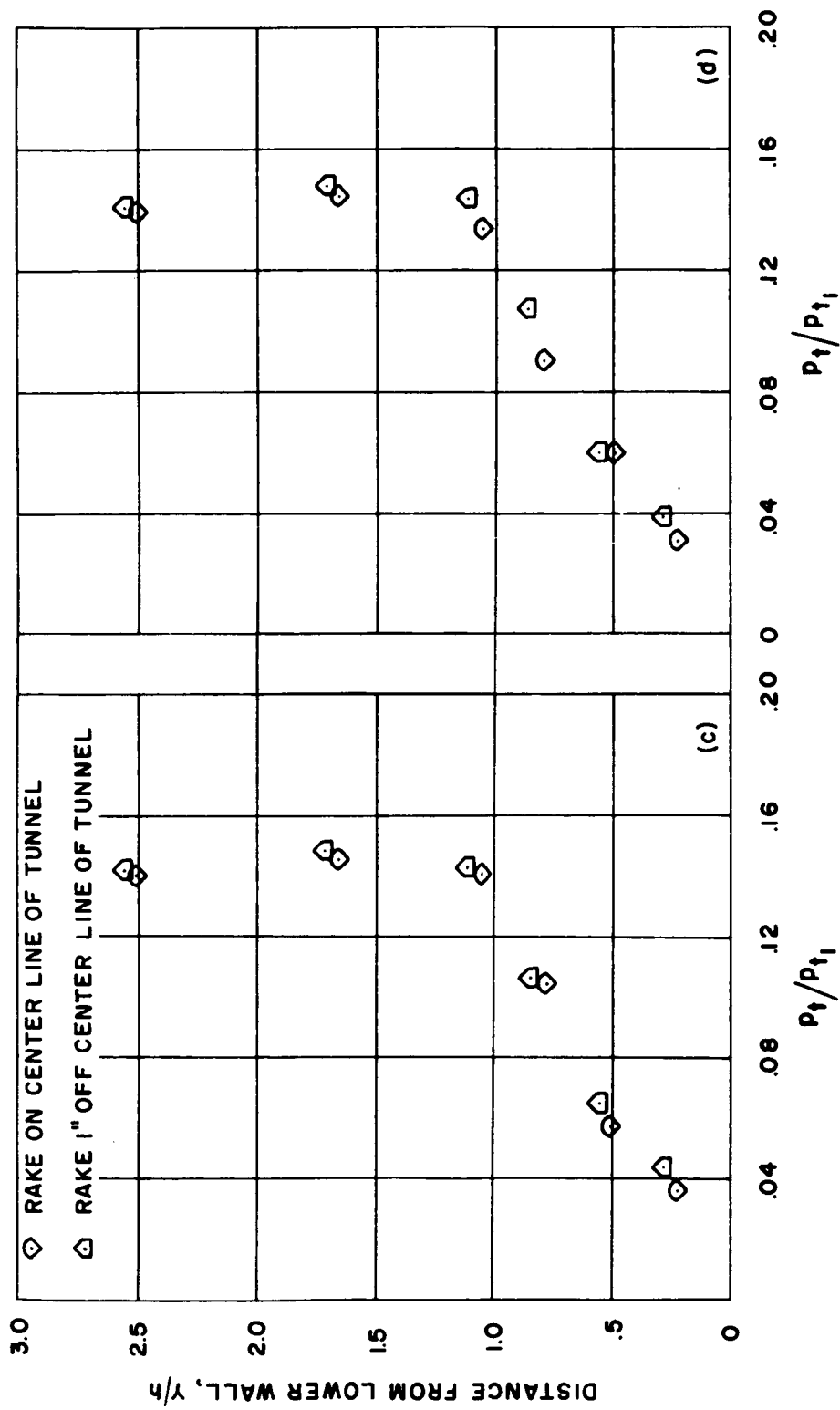
Figure 5.- Static-pressure distribution across the channel.



(a)  $\bar{M}_2 = 0$ .

(b)  $\bar{M}_2 = 0.14$ .

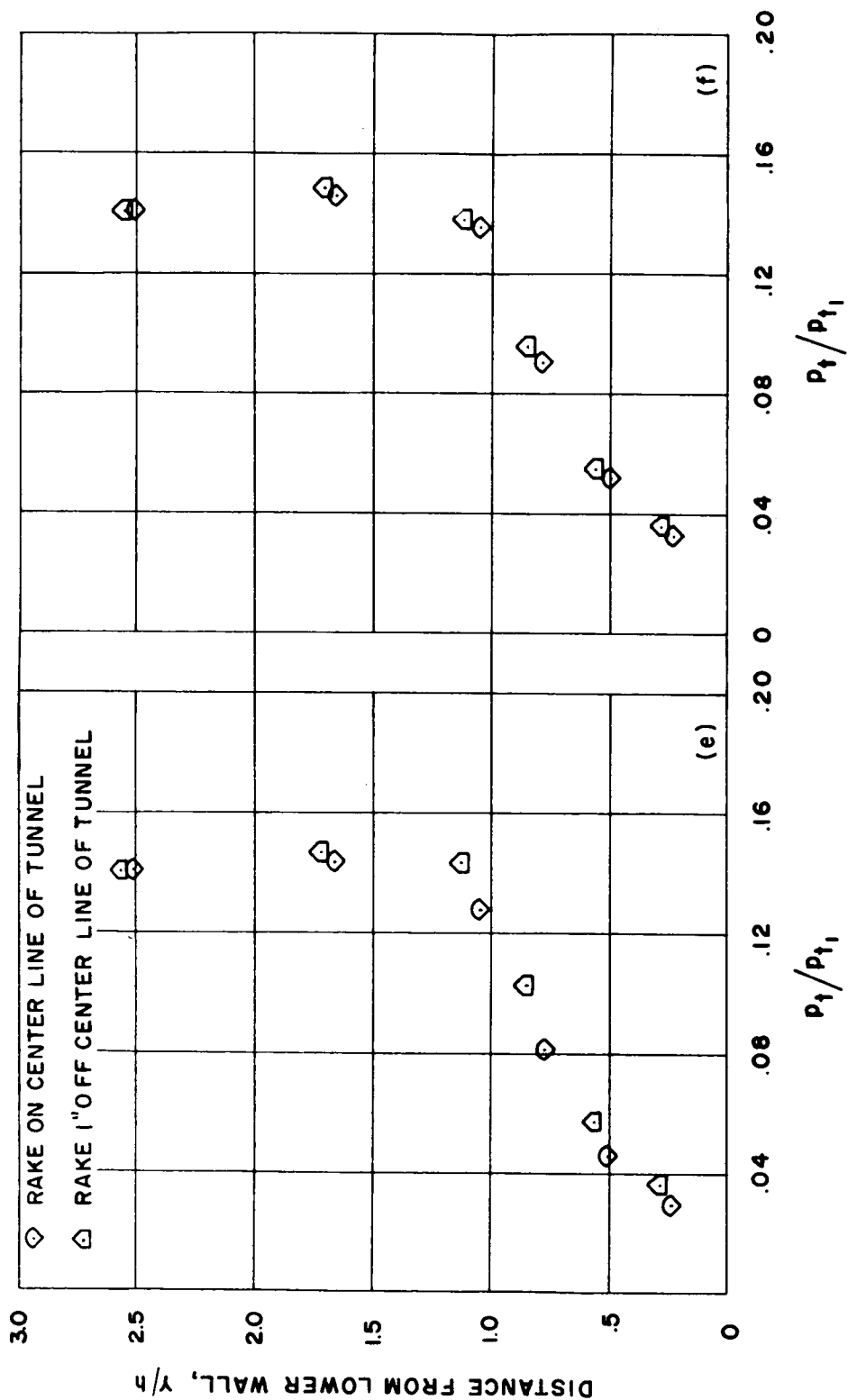
Figure 6.- Total-head surveys showing two-dimensionality of flow for  $x/h = 29.42$ .



(c)  $\bar{M}_2 = 0.20$ .

(d)  $\bar{M}_2 = 0.32$ .

Figure 6.- Continued.



(e)  $\bar{M}_2 = 0.36$ .

(f)  $\bar{M}_2 = 0.44$ .

Figure 6.- Concluded.

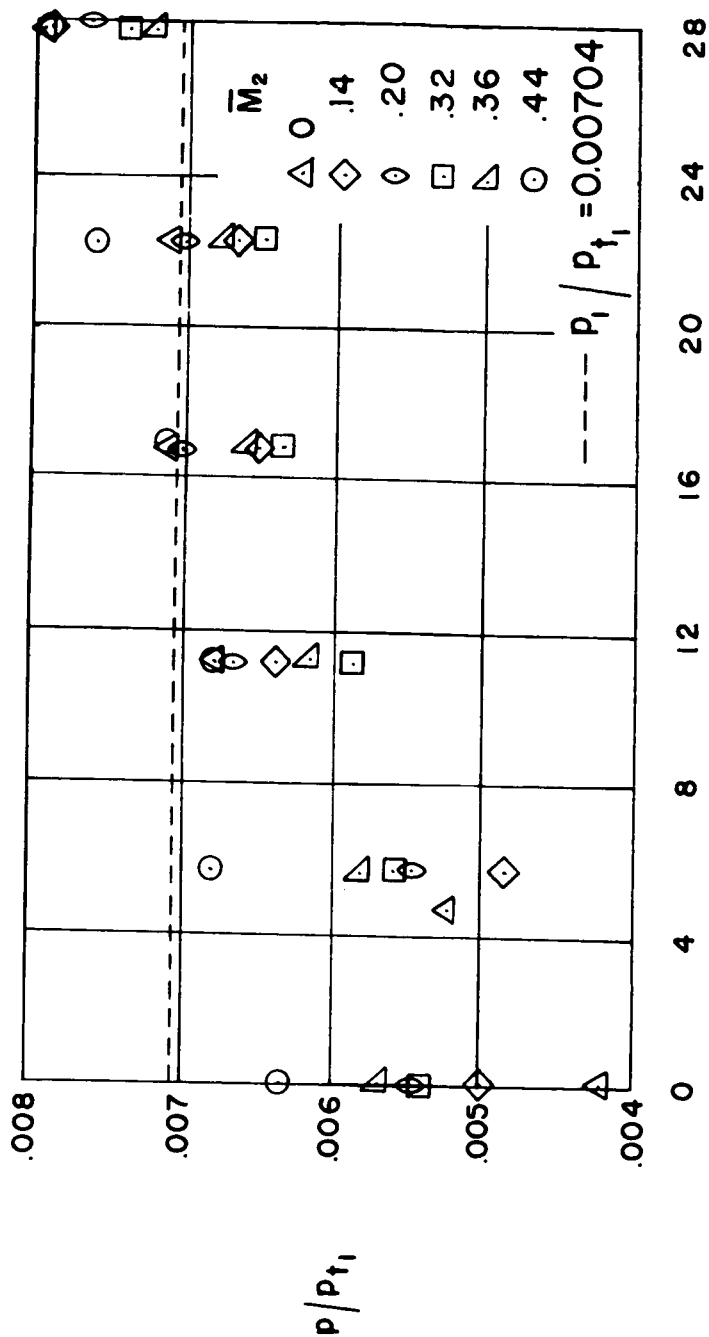


Figure 7.- Pressure distribution along lower wall for various secondary mass flows.

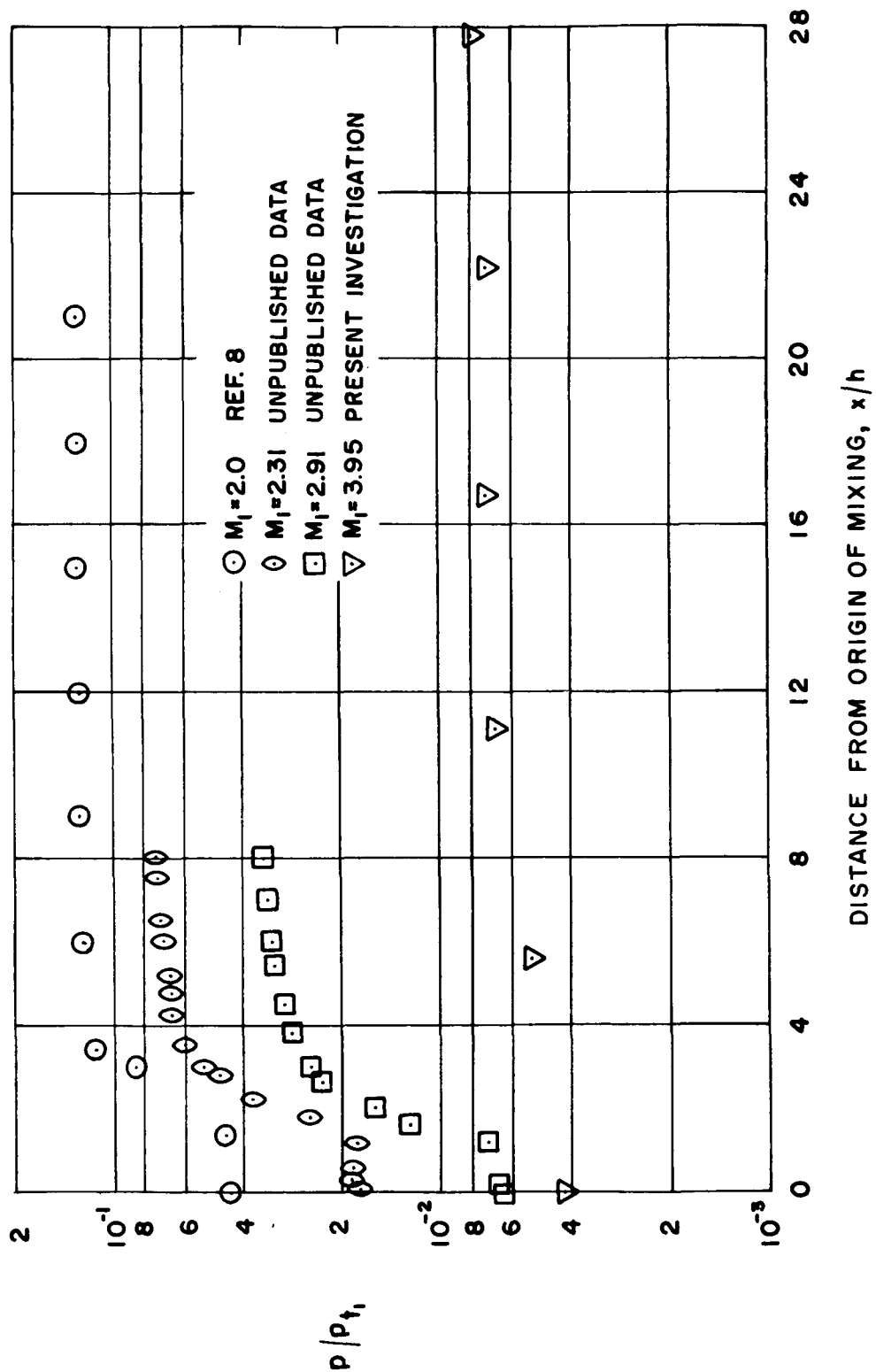


Figure 8.- Pressure distribution along lower wall for zero secondary mass flow and various values of free-stream Mach number.

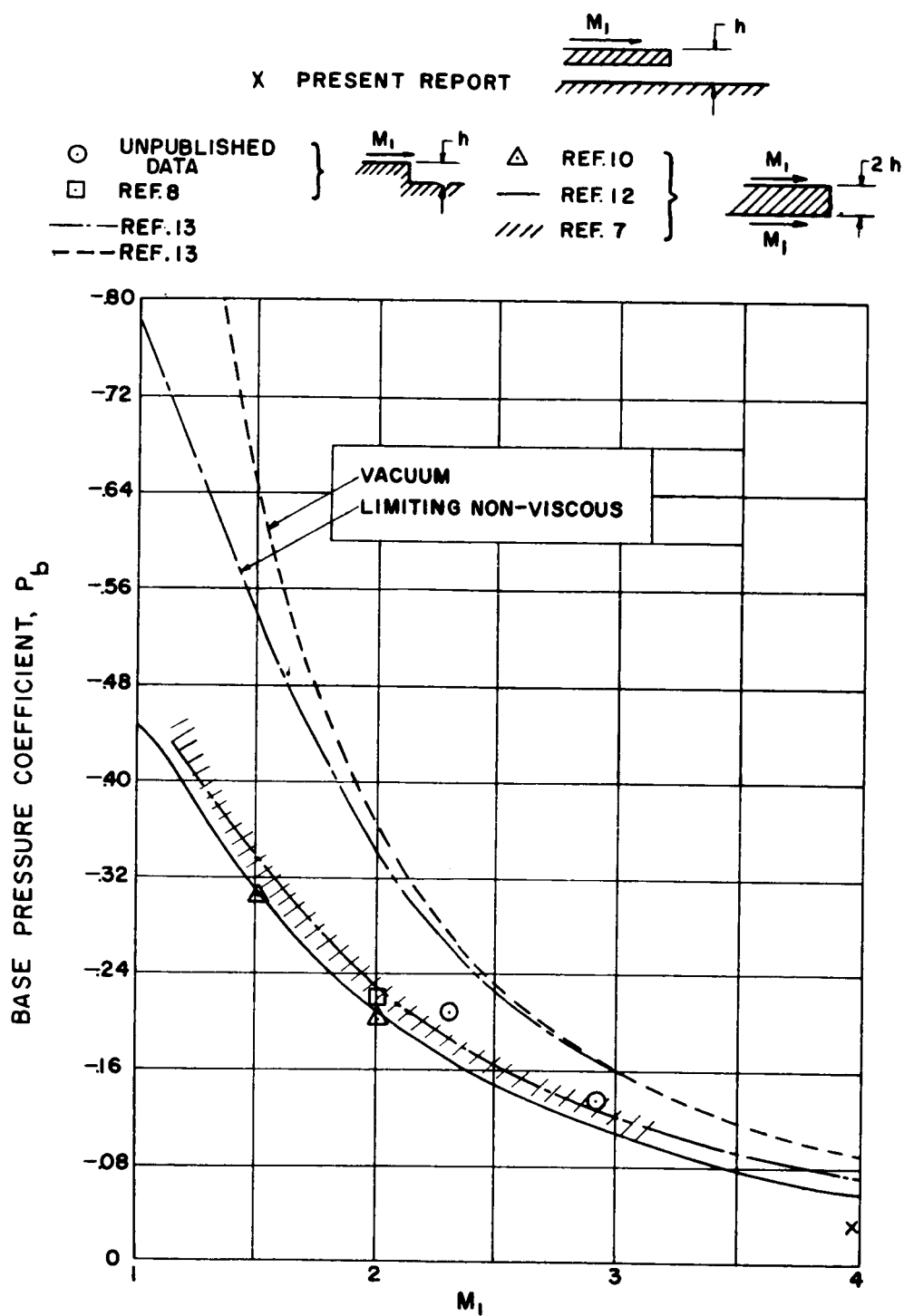


Figure 9.- Comparison of static pressure  $p_2$  with two-dimensional base pressure.

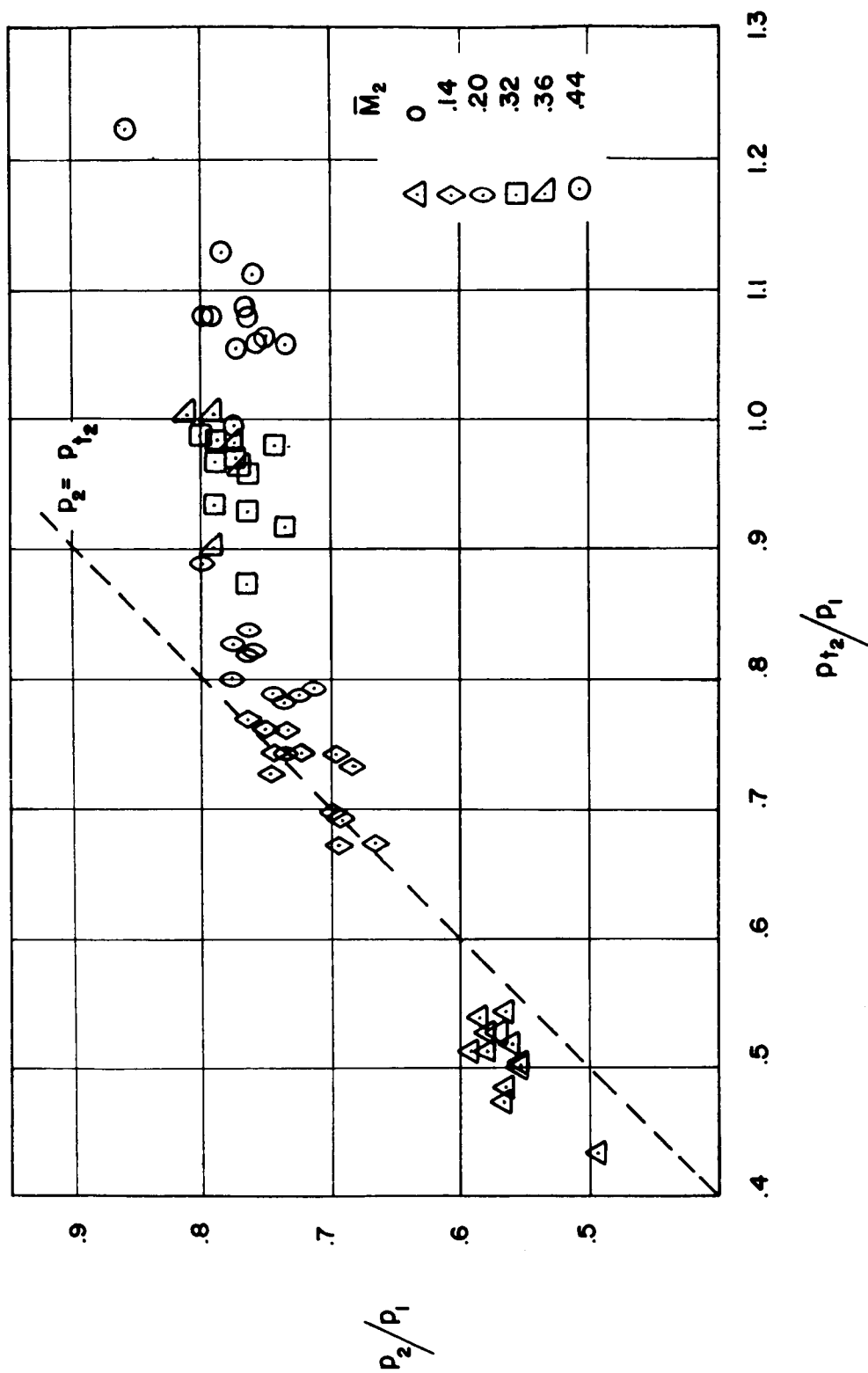
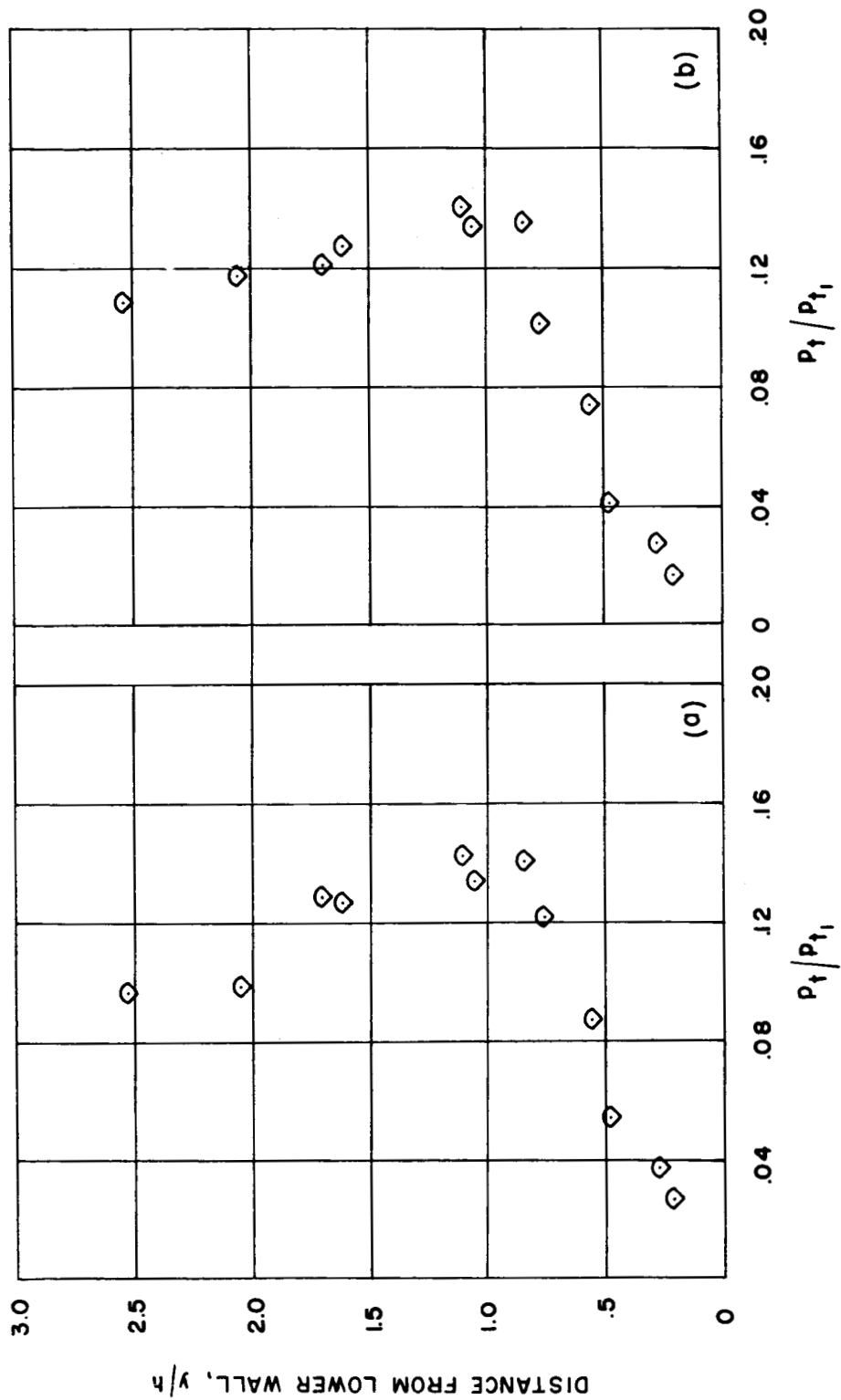
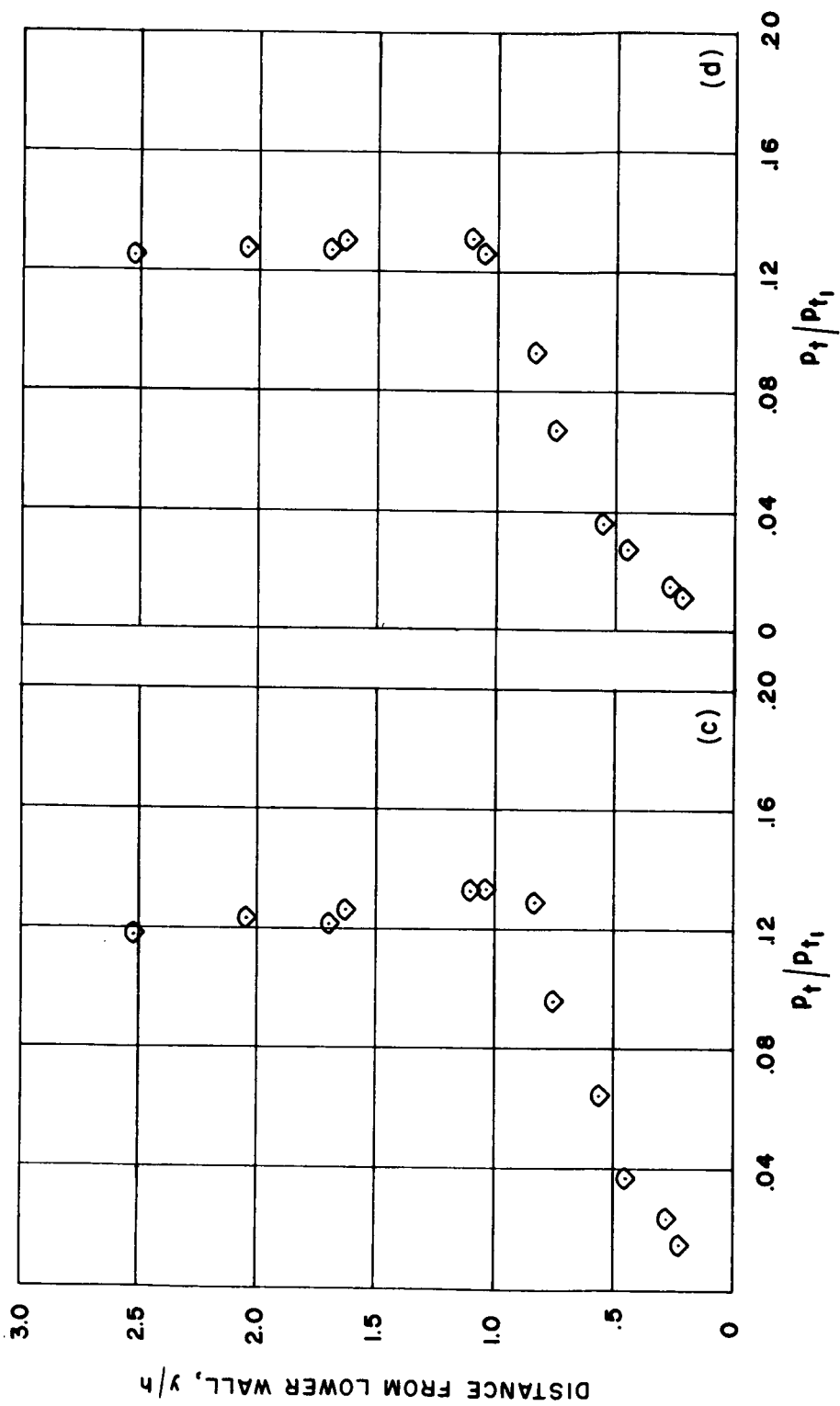


Figure 10.- Variation of static-pressure ratio with mean secondary Mach number.



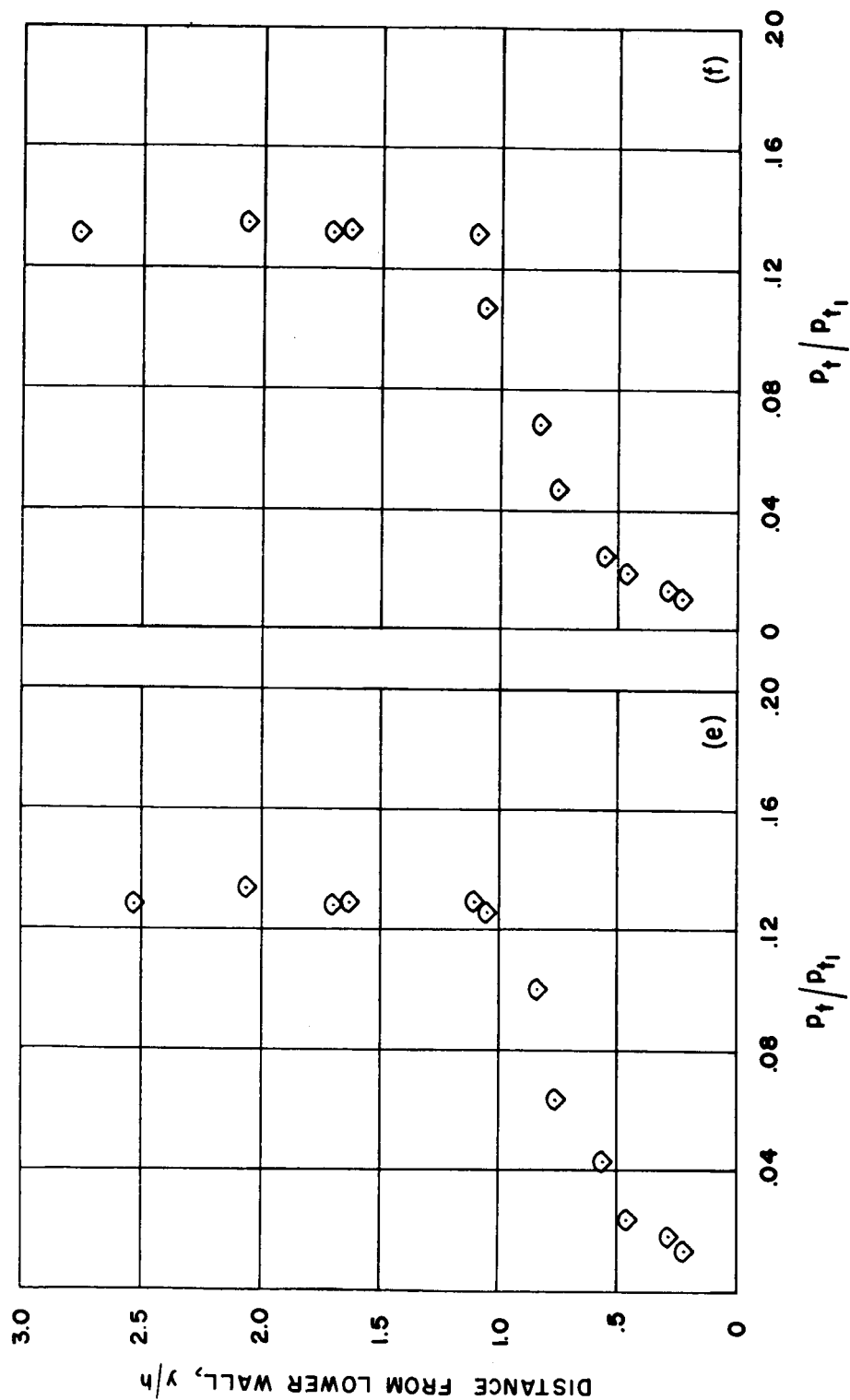
(a)  $x/h = 12.85$ ;  $\bar{M}_2 = 0$ . (b)  $x/h = 12.85$ ;  $\bar{M}_2 = 0.14$ .

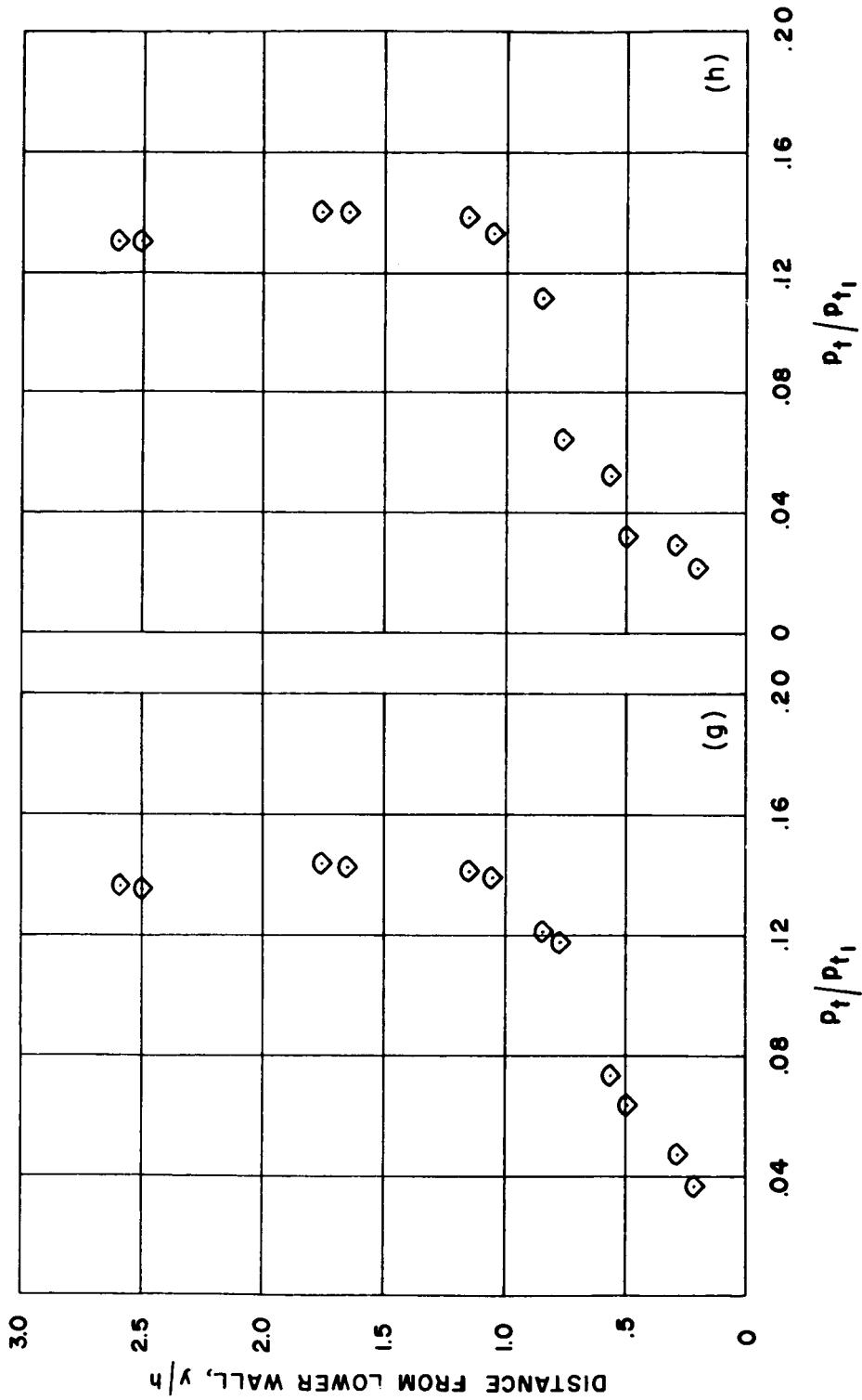
Figure 11.- Total-head profiles.



(c)  $x/h = 12.85$ ;  $\bar{M}_2 = 0.20$ . (d)  $x/h = 12.85$ ;  $\bar{M}_2 = 0.32$ .

Figure 11.- Continued.

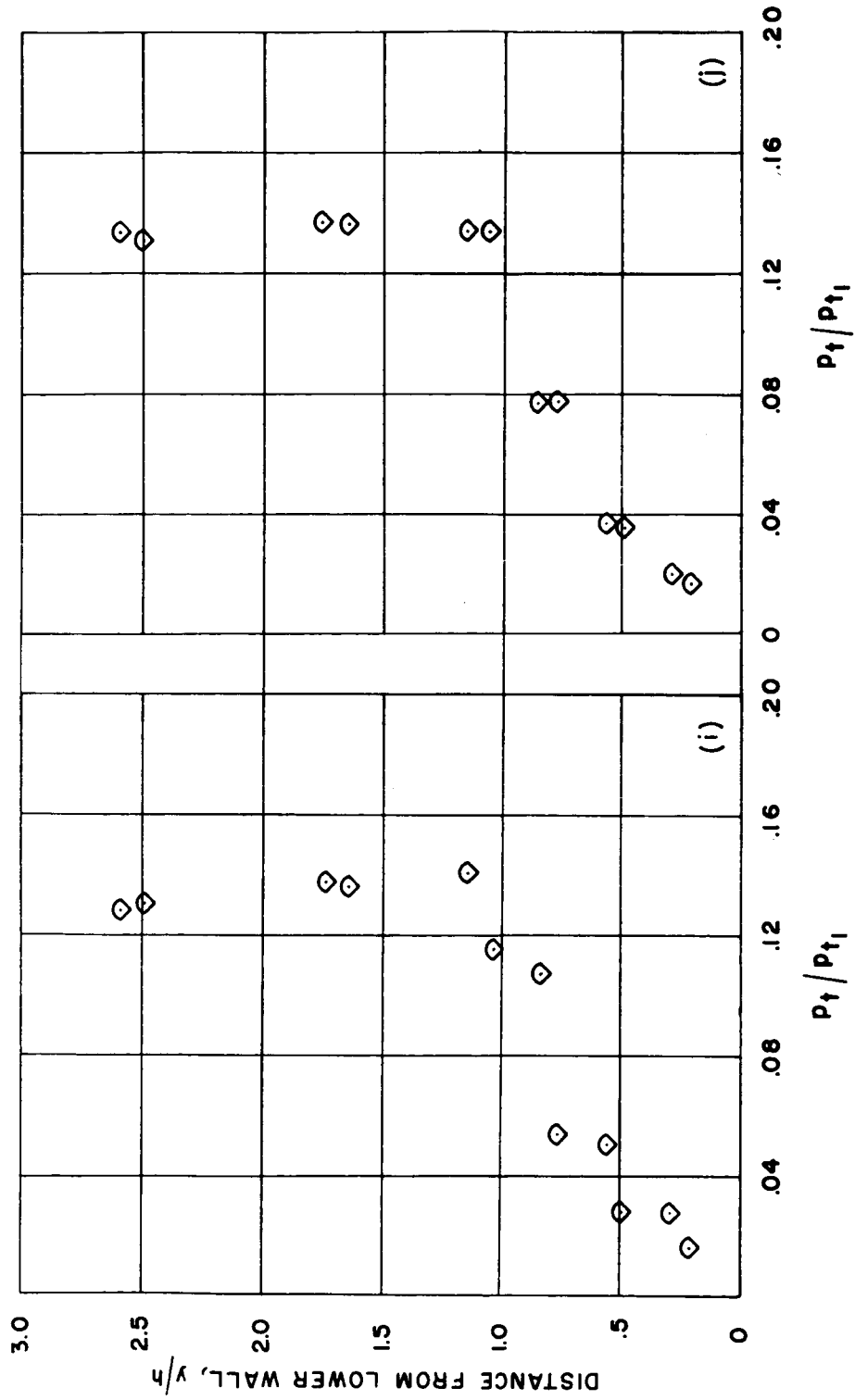




(g)  $x/h = 18.40$ ;  $\bar{M}_2 = 0$ .

(h)  $x/h = 18.40$ ;  $\bar{M}_2 = 0.14$ .

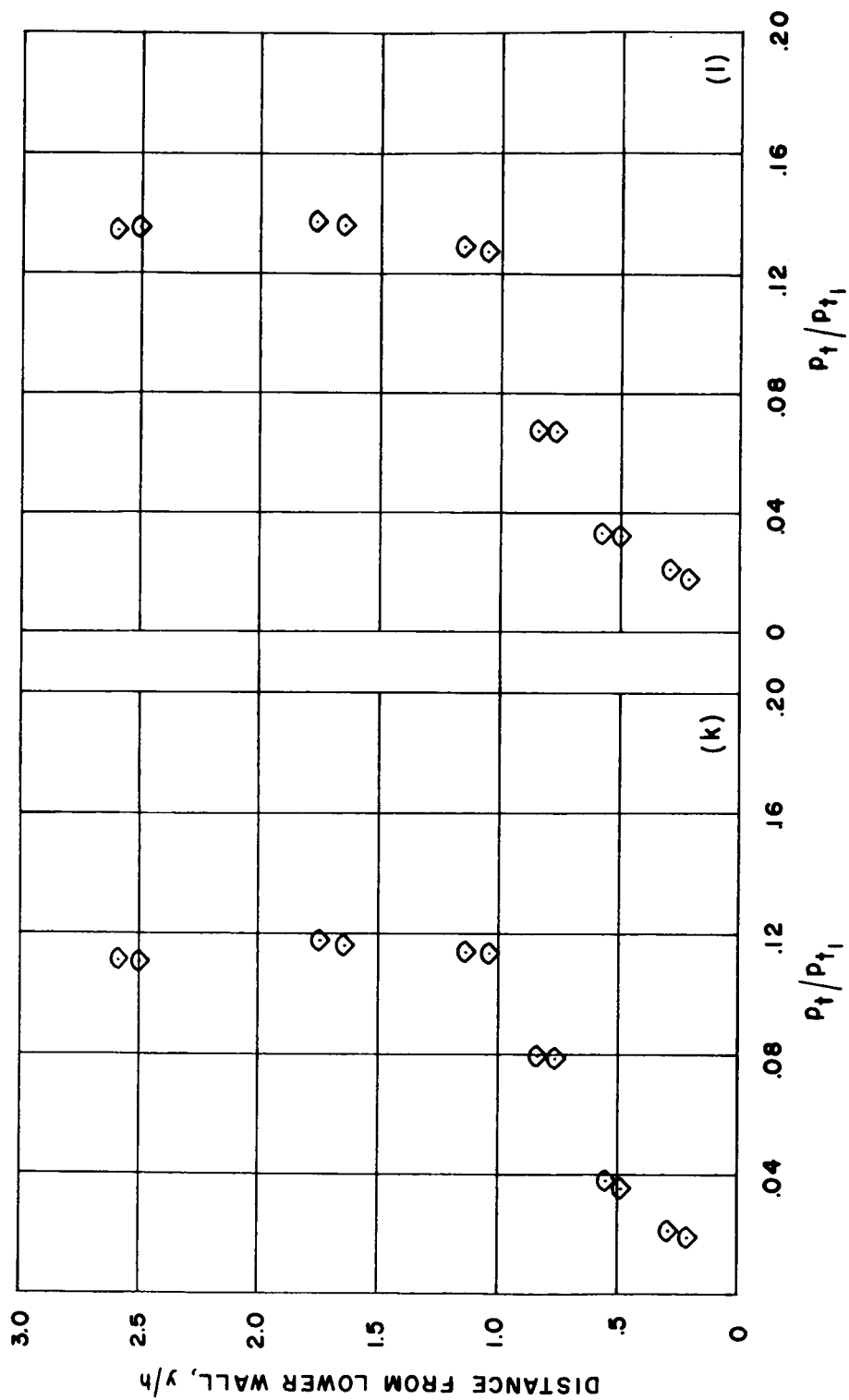
Figure 11.- Continued.



(i)  $x/h = 18.40$ ;  $\bar{M}_2 = 0.20$ .

(j)  $x/h = 18.40$ ;  $\bar{M}_2 = 0.32$ .

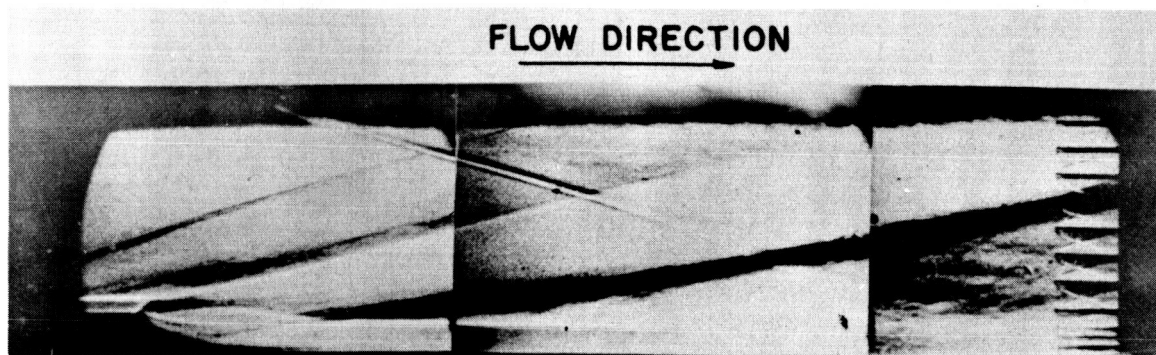
Figure 11.- Continued.



(k)  $x/h = 12.40$ ;  $\bar{M}_2 = 0.36$ .

(l)  $x/h = 12.40$ ;  $\bar{M}_2 = 0.44$ .

Figure 11.- Concluded.



(a)  $\bar{M}_2 = 0.$



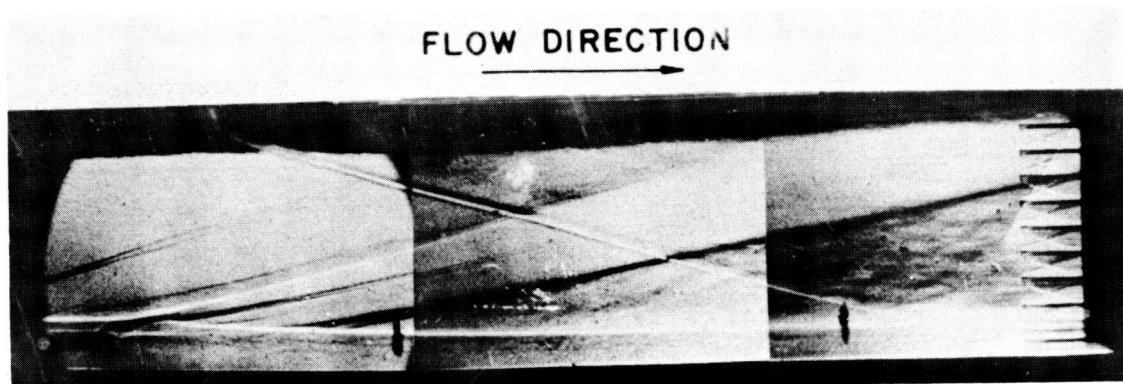
(b)  $\bar{M}_2 = 0.14.$



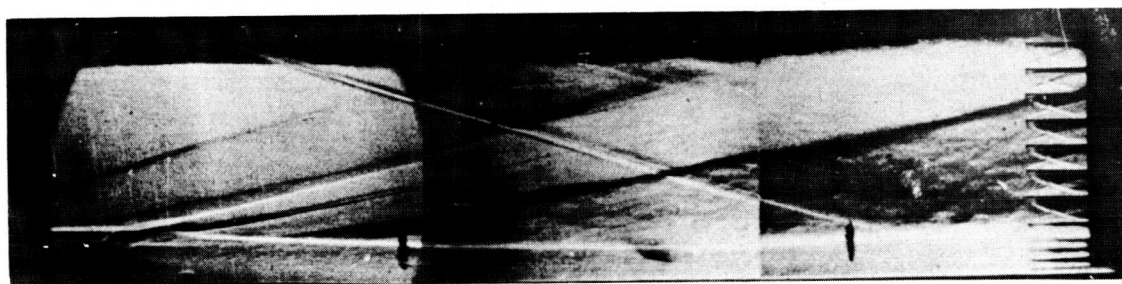
(c)  $\bar{M}_2 = 0.20.$

L-59-6471

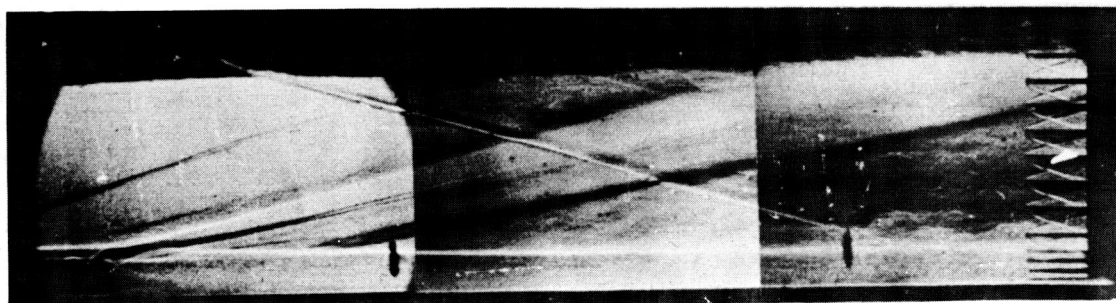
Figure 12.- Schlieren photographs of flow field.



(d)  $\bar{M}_2 = 0.32$



(e)  $\bar{M}_2 = 0.36.$



(f)  $\bar{M}_2 = 0.44.$

L-59-6472

Figure 12.- Concluded.

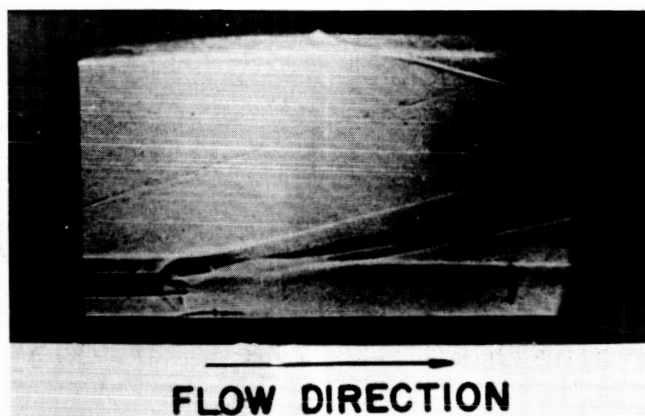
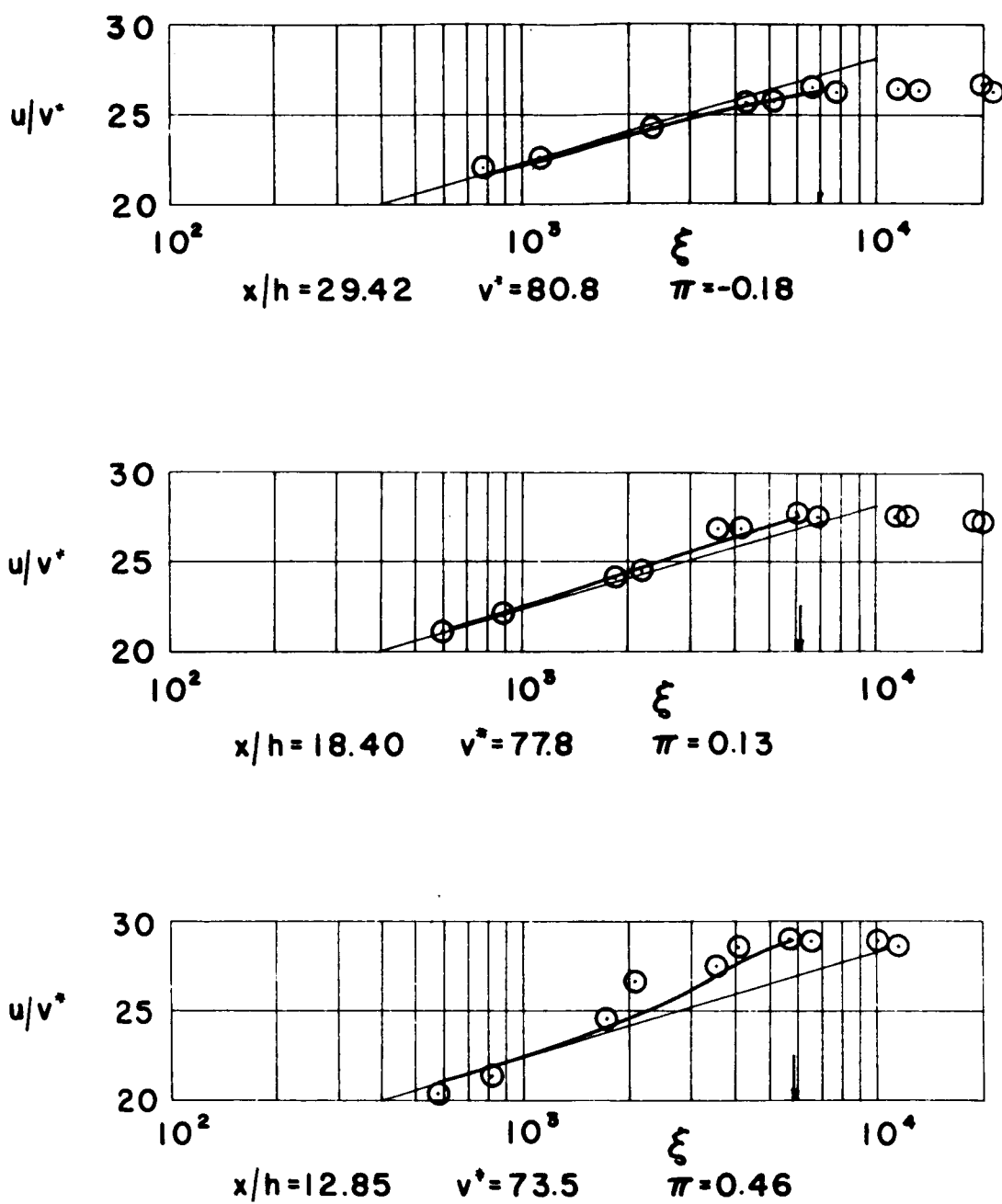


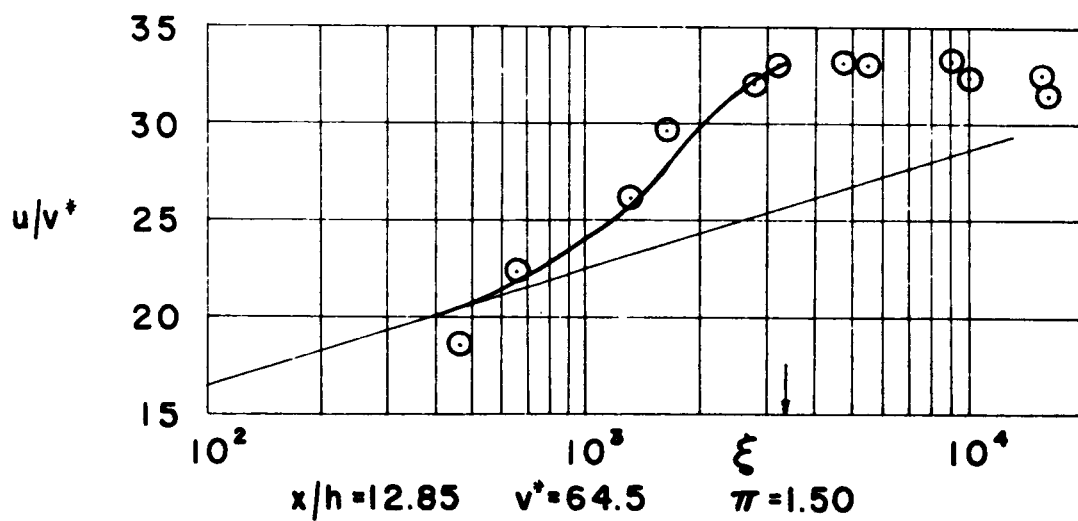
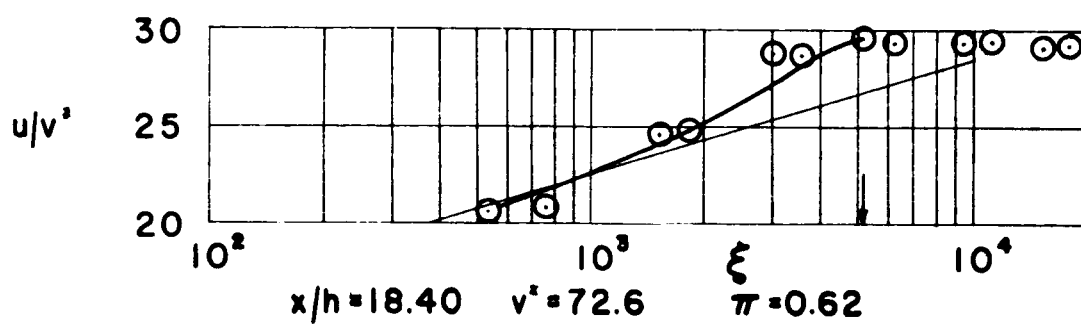
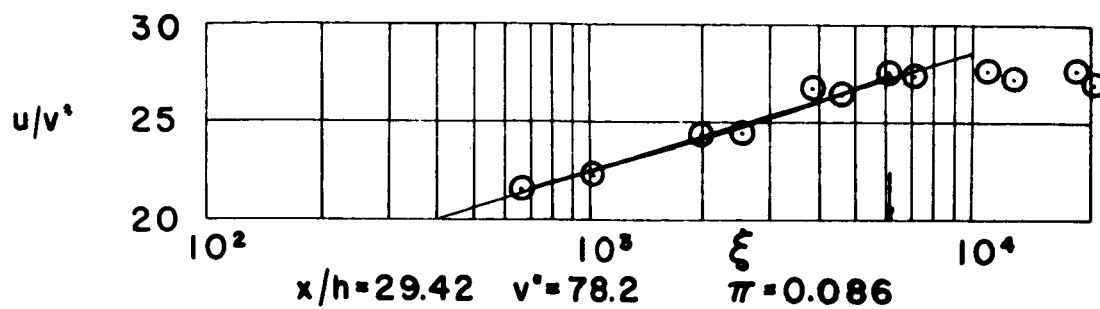
Figure 13.- Schlieren photograph of origin of mixing showing transonic effects at  $\bar{M}_2 \approx 0.50$ . L-59-6473

W-132



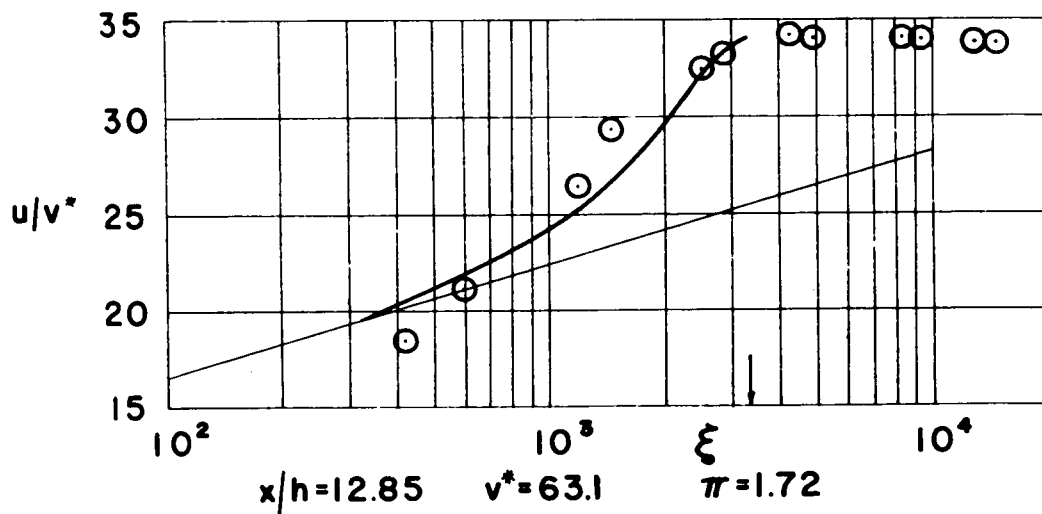
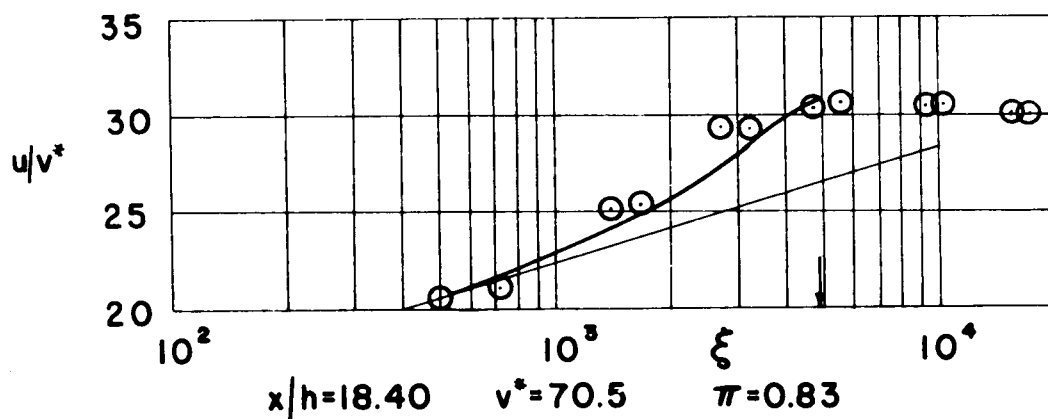
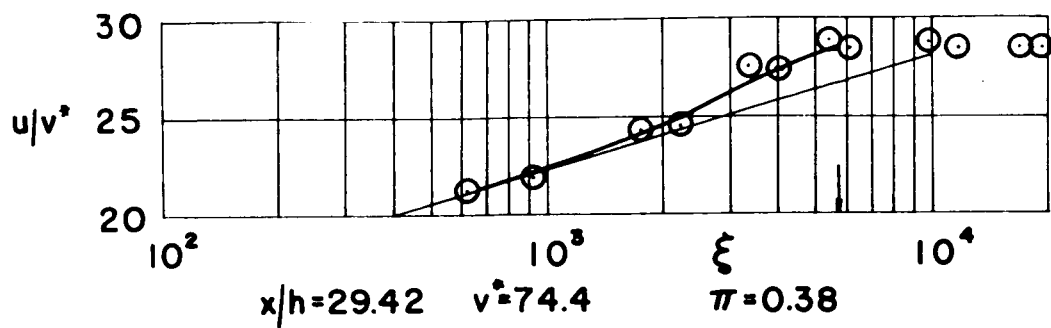
(a)  $\bar{M}_2 = 0$ .

Figure 14.- Velocity profiles.



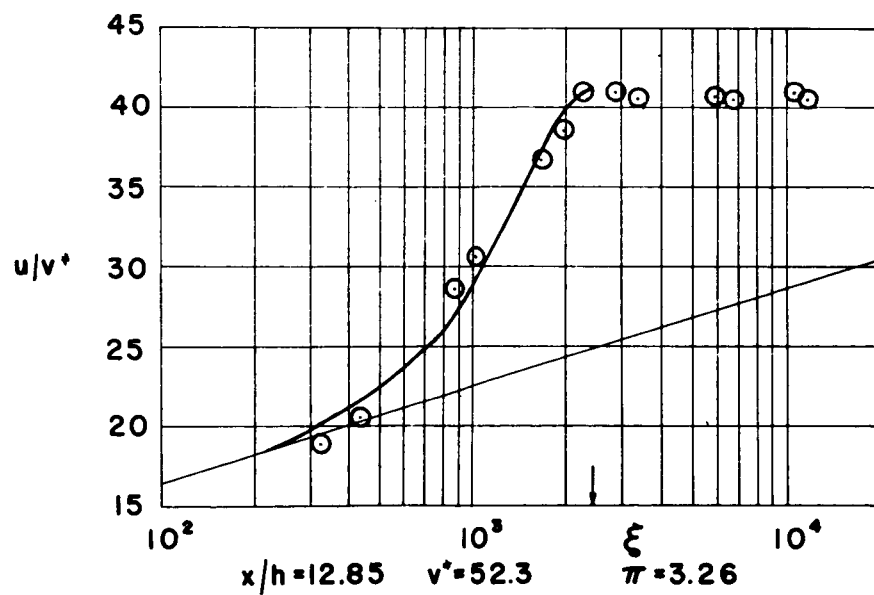
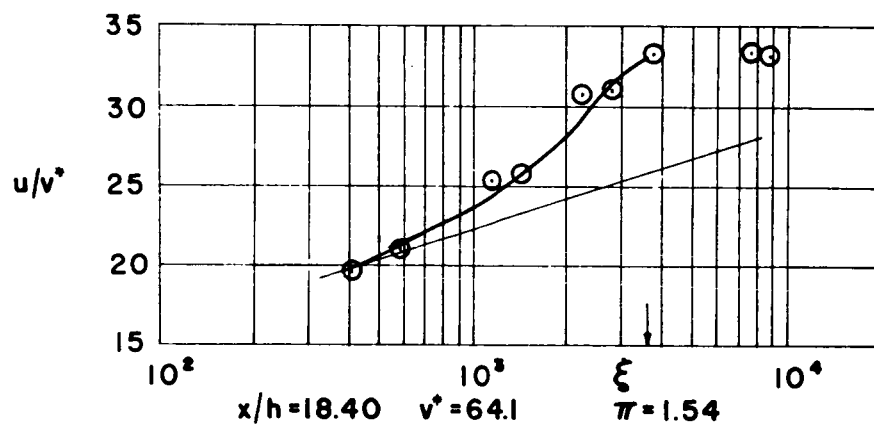
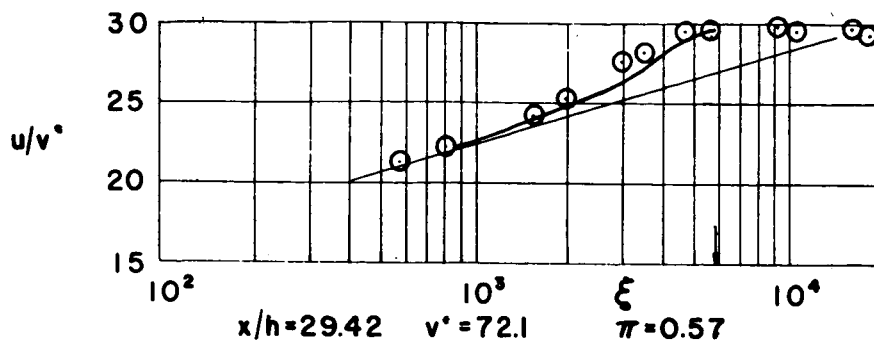
(b)  $\bar{M}_2 = 0.14$ .

Figure 14.- Continued.



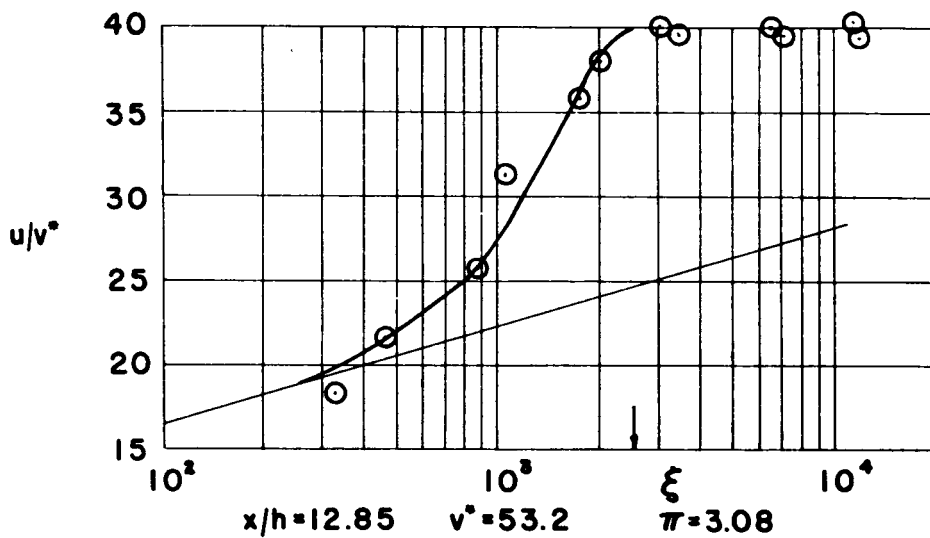
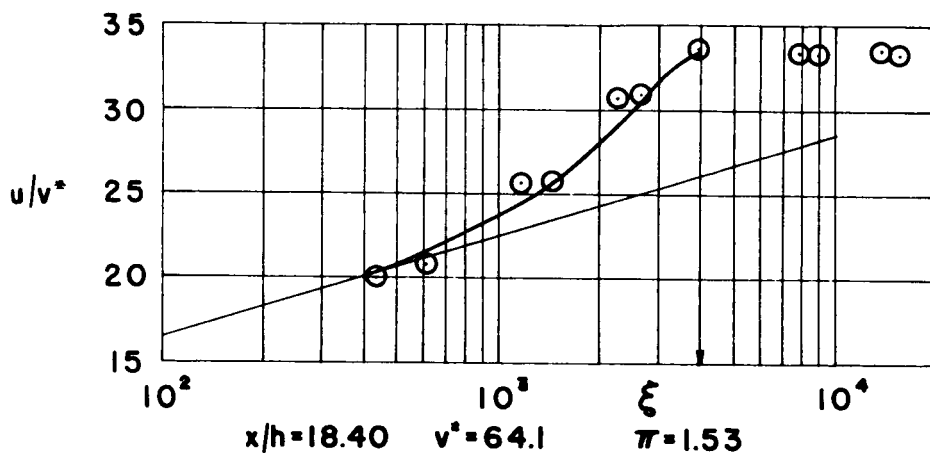
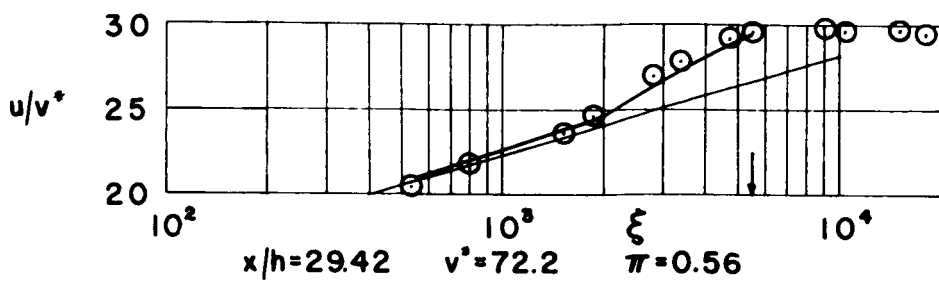
(c)  $\bar{M}_2 = 0.20$ .

Figure 14.- Continued.



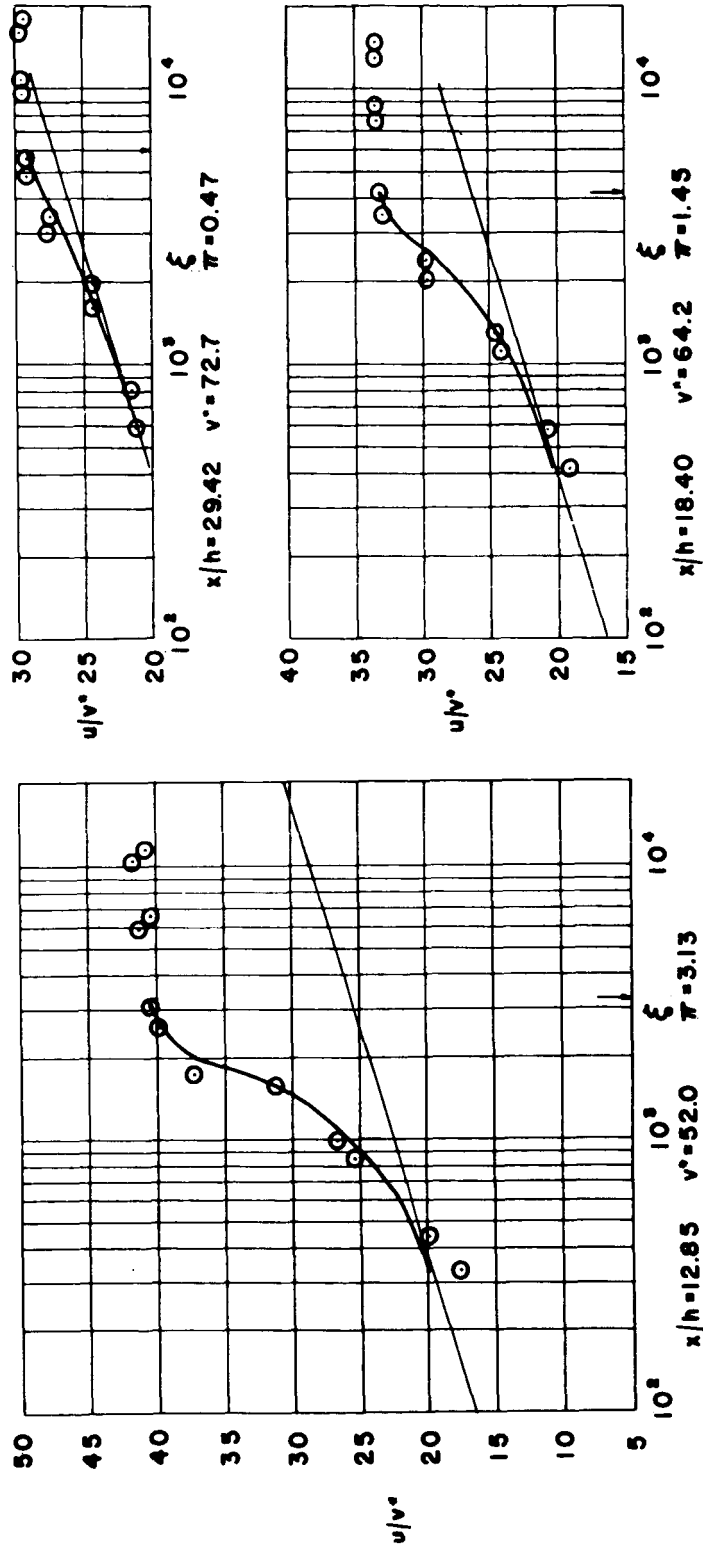
(d)  $\bar{M}_2 = 0.32$ .

Figure 14.- Continued.



(e)  $\bar{M}_2 = 0.36$ .

Figure 14.- Continued.



(f)  $\bar{M}_2 = 0.44$ .

Figure 14.- Concluded.

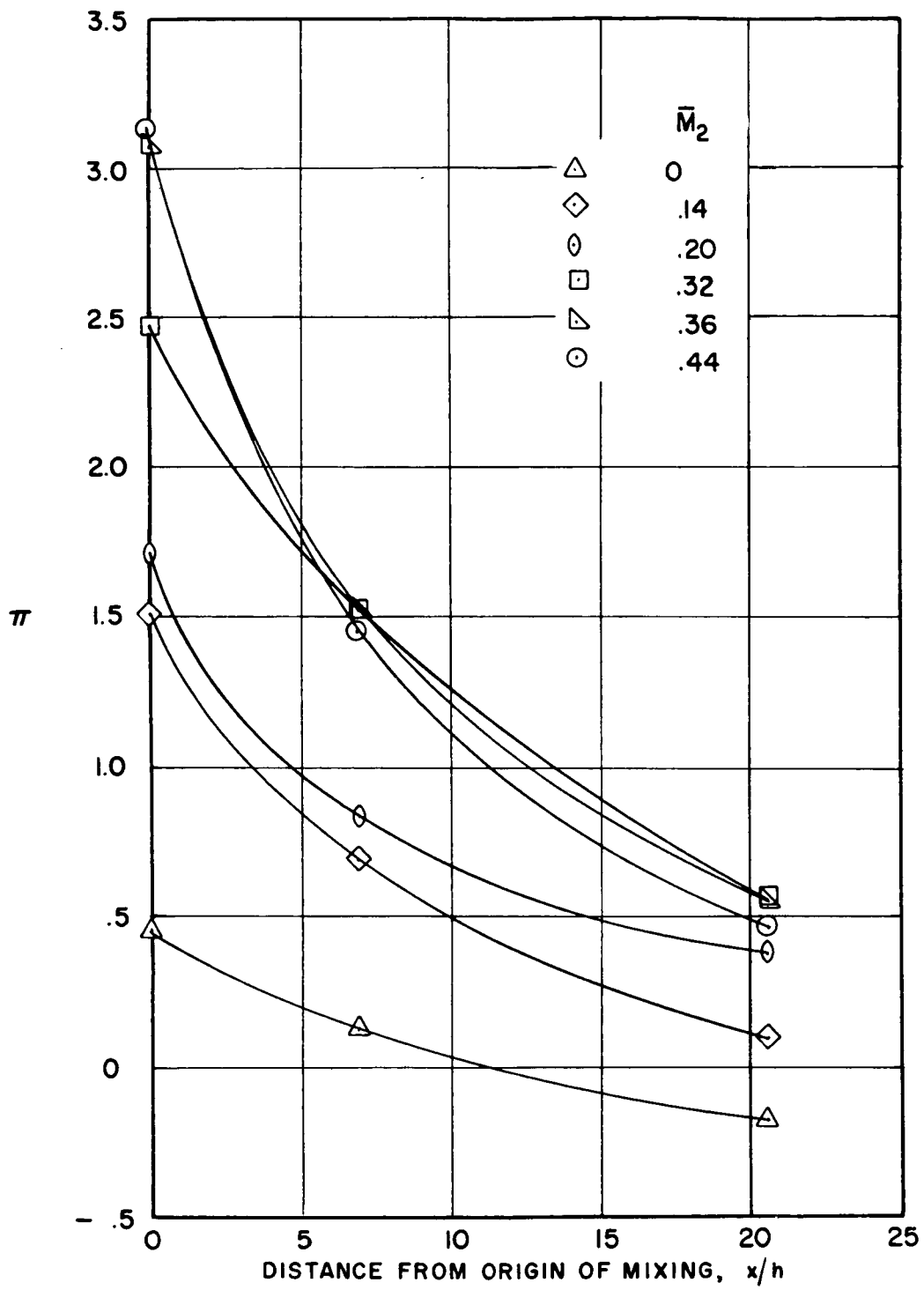


Figure 15.- Distribution of  $\pi$  in streamwise direction.

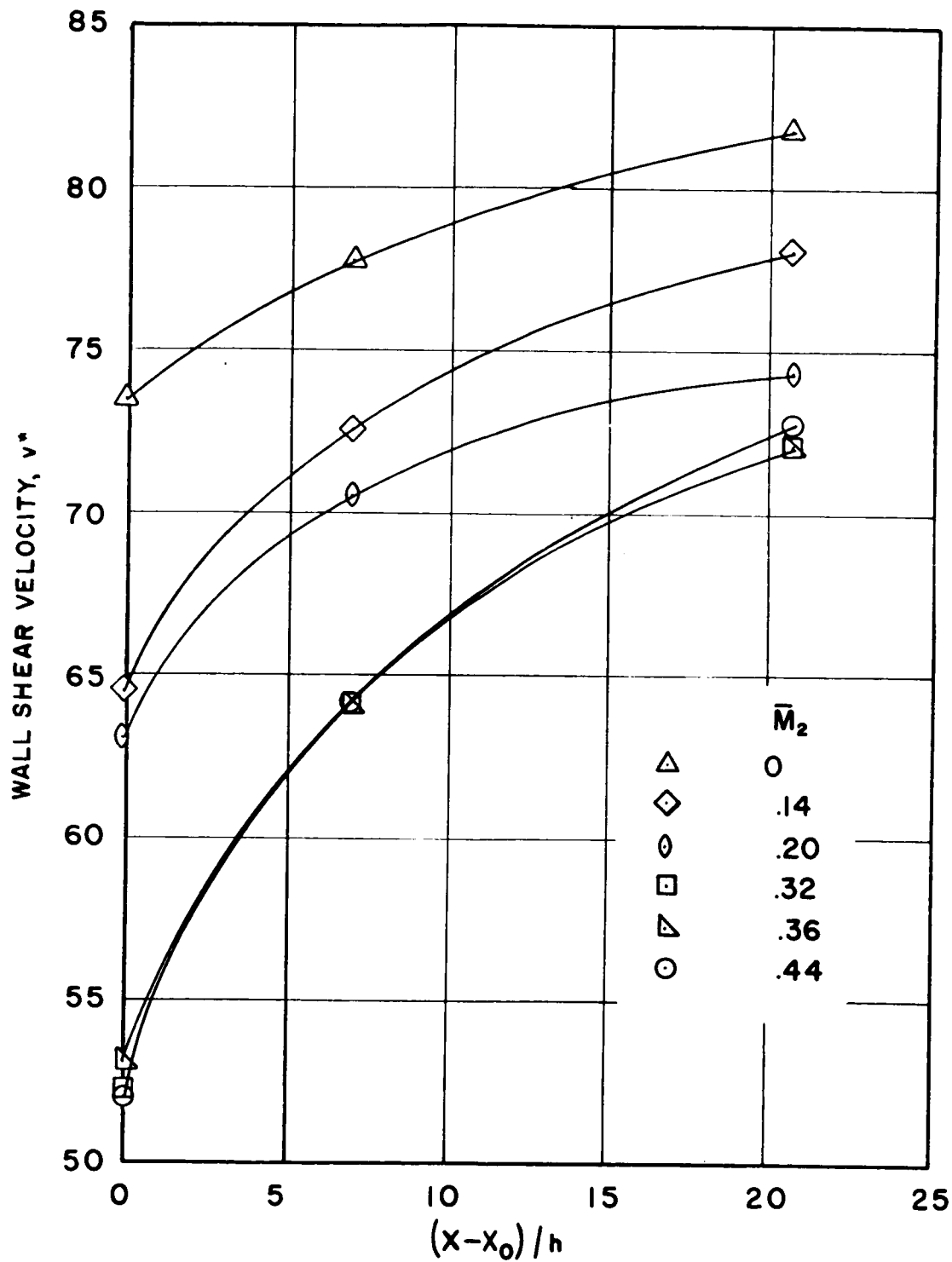


Figure 16.- Distribution of wall shear velocity in streamwise direction.